Top-storey softening for enhanced mitigation of vortex shedding induced vibrations in wind-excited optimal tuned mass damper inerter (TMDI)-equipped tall buildings

Zixiao Wang[1], Agathoklis Giaralis[2]*

* Corresponding author

[1] PhD Candidate, Department of Civil Engineering, City, University of London, UK
e-mail:zixiao.wang@city.ac.uk
[2] Senior Lecturer, Department of Civil Engineering, City, University of London, UK
e-mail: agathoklis@city.ac.uk

ABSTRACT

An innovative structural modification, top-storey softening, is herein proposed in conjunction with optimally tuned top-floor tuned mass damper inerter (TMDI) for improved serviceability performance in typical core-frame slender buildings with rectangular floor plan susceptible to wind-induced vortex shedding (VS) effects causing occupant discomfort. This is supported through formulating a novel optimal TMDI tuning problem in which TMDI inertial properties, i.e., attached mass and inertance, as well as the lateral top-storey stiffness are design parameters aiming to minimize peak acceleration of the highest occupied floor. The optimal TMDI tuning problem is numerically solved for a wide range of design parameters for a 34-storey composite core-frame building subject to stochastic spatially-correlated wind-force field accounting for VS effects. A low-order dynamical model capturing faithfully modal properties of the case-study building is developed to facilitate computational work and parametric investigation. It is found that top-storey softening reduces attached TMDI mass/weight requirements and inerter force for fixed performance and inertance. It further reduces TMDI stroke and achieves increased robustness to TMDI stiffness and damping properties as well as to the assumed inherent structural damping. It is concluded that by leveraging inertance and top-storey stiffness, the proposed solution can efficiently control VS-induced floor acceleration with small additional gravitational (added weight) and horizontal (inerter and damping) forces.

Keywords: *tuned mass damper, inerter, passive vibration control, wind-excited tall buildings, vortex shedding, low-order modeling, floor acceleration.*

INTRODUCTION AND MOTIVATION

Continuous increasing cost of land in congested metropolitan areas as well as sustainability requirements in construction industry have been driving recent trends for designing and erection of slender high-rise buildings with high aspect ratios and rectangular floor plans achieving efficient land usage and internal space organization. Nevertheless, such structures are prone to excessive oscillations in the across-wind direction (i.e., within the normal plane to the wind direction) due to vortex shedding (VS) effects generated around their corner edges (Liang et al. 2002) and due to low inherent damping (Spence and

Kareem 2014). Consequently, their design is usually governed by serviceability performance criteria, namely ensuring that floor accelerations in the across-wind direction are below thresholds related to occupants' comfort prescribed by building codes and guidelines (Burton et al. 2006, Kwok et al. 2009, Petrini and Ciampoli 2012, Taranath 2017). These design requirements are often met in practice by employing vibration control devices since increasing the lateral stiffness of tall buildings does not mitigate efficiently VS-induced floor accelerations (e.g., Huang 2017).

To this effect, passive tuned mass-dampers (TMDs) have been widely used, among other energy dissipation devices and configurations, for mitigating wind-induced vibrations in tall buildings (e.g., Kareem et al. 1999, Samali et al. 2004, Min et al 2005, Li et al. 2011, Elias and Matsagar 2014, Zhang et al. 2018, Elias and Matsagar 2018). A typical linear TMD comprises a mass attached towards the top of the building (host structure) via linear stiffeners, or hangers in case of pendulum-like TMD implementations, and dampers. For a pre-specified attached mass, motion control of the host structure is achieved by tuning the TMD stiffness and damping properties such that significant kinetic energy is transferred from the wind-excited building to the TMD mass and eventually dissipated through the dampers. In principle, the TMD is tuned to the first natural frequency of the building aiming to dampen the fundamental lateral mode shape which tends to resonate with the frequency of VS-induced forces (e.g., Ciampoli and Petrini 2012). Then, the potential of TMD for vibration suppression depends on its inertia: the larger the attached TMD mass is, the more effective and robust to uncertainties in the structural building properties and detuning effects the TMD becomes (De Angelis et al. 2012). However, practical structural and architectural constraints apply to the TMD weight and volume that can be accommodated at the top floor of slender/tall buildings while TMD up-front cost is proportional to the attached mass (Tse et al. 2012).

To overcome the above TMD limitations, Giaralis and Petrini (2017) recently explored the potential of top-storey tuned mass damper inerter (TMDI), originally proposed for mitigating earthquake induced vibrations in multi-storey buildings (Marian and Giaralis 2013, 2014), to enhance TMD vibration suppression effectiveness in wind-excited tall/slender structures subject to VS effects without increasing the attached mass. The TMDI is composed of a conventional linear passive TMD in which the attached mass is linked to *a different floor* from the one that the TMD is attached to via an *inerter* element/device (Fig. 1(b)). The latter is conceptually defined by Smith (2002), as a linear massless mechanical element developing a force proportional to the relative acceleration by the so-called *inertance* coefficient of proportionality, b, as shown in the inlet of Fig.1(b). Giaralis and Petrini (2017) showed that the TMDI achieves appreciably larger peak top floor acceleration reductions compared to the TMD for same attached mass in a wind-excited 74-storey benchmark building as the inertance increases and/or as TMDI topologies with the inerter spanning more than one storey are considered. The latter consideration is graphically explained in Figs. 1(b) and 1(c) showing two different TMDI topologies in a *n*-storey building with the inerter spanning one (the top) storey ("-1" topology) and two (the top and the penultimate) storeys ("-2" topology), respectively. Moreover, Fig. 1(e) furnishes

indicative numerical data (explained and discussed in detail later in the paper) demonstrating that transfer function ordinates of the *n*-2 floor acceleration reduce for optimally designed TMDIs with topology "-2" vis-à-vis "-1" for the same attached mass and inertance (see also Giaralis and Taflanidis 2015 and 2018).
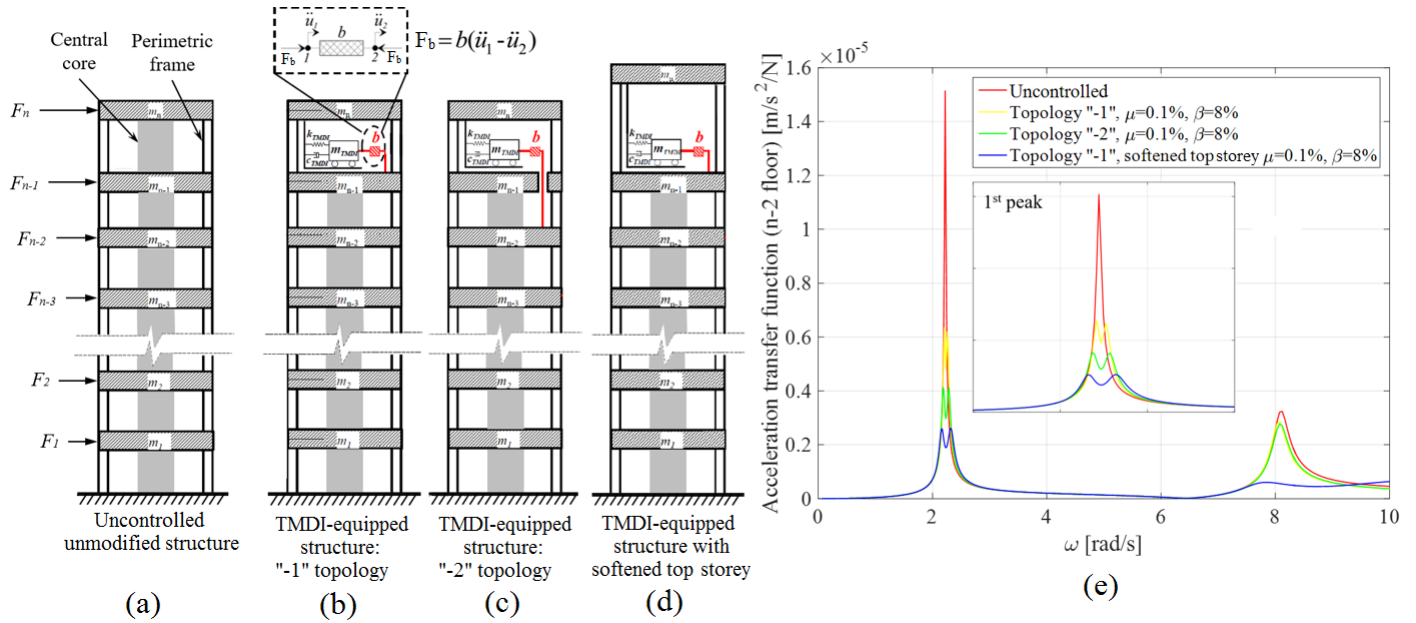

Fig. 1. (a) Planar graphical representation of a typical coupled core-frame building (primary structure), (b) and (c) Unmodified primary structure with different TMDI topologies, (d) Proposed structural modification with top-storey TMDI, (e) Floor acceleration transfer functions for uncontrolled and TMDI-controlled structures.

Nevertheless, it is found that the improved floor acceleration performance came at the expense of larger inerter force exerted to the building structure for increased inertance and/or for TMDI topologies spanning more floors (Giaralis and Petrini 2017, Petrini et al. 2020). More importantly, it is herein recognized that whilst TMDI topologies with inerter spanning more than one floor may be economically feasible for land-mark structures/skyscrapers with large number of storeys featuring large slab openings and, possibly, pendulum-like TMDI implementations (see e.g., Li et al 2011 discussing Taipei 101 skyscraper), it does not seem a practically sensible solution for the typical, and quite popular, slender mid-to-high-rise residential buildings with 20-40 storeys and rectangular floor-plans. This is because sacrificing high-premium space in the top floors of such structures, apart from the last floor commonly accommodating various services, to contain VS-induced floor accelerations is not cost-efficient.

To this end, for the case of routine slender buildings with 20-40 storeys and rectangular floor-plans, this paper proposes a novel structural modification, namely top-storey softening, in conjunction with a top-storey TMDI in "-1" topology placement as graphically shown in Fig.1(d) to mitigate floor accelerations in the across-wind direction in an efficient and cost-effective manner. Specifically, note that the typical lateral load-resisting structural system of the considered buildings comprises a reinforced concrete (r/c) core coupled with perimetric moment resisting frames (MRFs) as depicted in Fig.1(a) (e.g., Taranath

2017). Then, top-storey softening can be readily implemented by discontinuing the r/c core beyond the penultimate floor/slab and, if required, by further reducing the top-storey lateral stiffness. The latter may be accomplished by increasing the top-storey height, as shown in Fig.1(d), among other alternative approaches such as size reduction of top-storey structural members. From the structural dynamics viewpoint, consideration of top-storey softening is motivated by the fact that reducing the lateral stiffness of the storey equipped with the TMDI has, phenomenologically, similar effects to system transfer function as letting the inerter of the TMDI span more floors while keeping in all cases TMDI weight and inertance fixed as evidenced in Fig. 1(e).
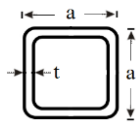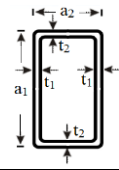
In this context, the aim of this work is to quantify gains (reduction) in peak floor accelerations in coupled core-frame buildings subject to VS effects equipped with TMDI ("-1" topology) as the top-storey softens. Attention is focused on various practical considerations such as attached mass/weight requirements, TMDI forces transferred to the building, attached mass deflection/stroke demands, as well as performance robustness to TMDI and to building properties. In exploring the above aspects, a novel optimal design problem is formulated for top-floor-TMDI-equipped structures with purposely softened top-floor in which TMDI inertial properties (attached mass and inertance) as well as the lateral stiffness of the top floor are treated as design parameters such that the proposed local structural modification (top-floor softening) becomes explicitly part of the optimal TMDI tuning problem. The developed optimization problem aims to minimize floor acceleration of the last occupied storey (n-2) (performance) instead of the top floor, as is usually considered in top-floor TMD(I) implementations, to ensure that top-floor softening does not create an artificially deficient host building structure while a fair and meaningful performance assessment compared to the unmodified structure can be made. The optimal design problem is numerically solved for a wide range of design parameters pertaining to a case-study 34-storey composite core-frame structure subject to an across-wind excitation model developed by Liang et al. (2002) to account for VS effects in tall buildings with rectangular floor plan. Parametric investigations are facilitated and computational work is expedited by developing a low-order linear dynamical model in terms of mass, stiffness, and damping matrices capturing modal properties of core-frame structures with different properties as detailed in the following.

CASE-STUDY COUPLED CORE-FRAME BUILDING AND FE MODELLING

The potential of top-storey softening for mitigating wind-induced vibrations in TMDI-equipped core-frame tall buildings is assessed throughout this work with reference to the 34-storey case-study structure shown in Fig.2(a). The adopted structure is 110.6m high and has rectangular 24m-by-24m footprint. The lateral load- resisting structural system is composite consisting of a perimetric steel MRF and a central reinforced concrete (r/c) core. The MRF has 12 equally-spaced columns in total and, therefore, three-bay frames with 8m opening are formed along each side of the building as shown in Fig.2(b). MRF members, columns and beams, are rigidly connected and have hollow rectangular sections with varying dimensions along the building height reported in Table 1. The r/c core has 8m-by-8m plan-view dimensions and comprises of outer and inner shear wall segments as seen in Fig.2(c). The thickness of

the outer r/c core walls decreases with building height as detailed in Table 1 while one large (door) opening is left within the y-z plane on each side of the core (Fig.2(c)). The inner (stiffening) shear wall segments have uniform thickness with building height (Table 1). The MRF and core are coupled at each floor level through primary beams assumed to be hinged at both ends. Therefore, primary beams carry only gravitational loads: they do not participate in resisting lateral loads and do not transfer moments to the MRF and core. Slabs are taken as rigid diaphragms.

Table 1. Member sections geometry of 34-storey composite core-frame case-study building

floor	storey height [m]	Hollow square column sections (a×t) [mm]	Hollow rectangular beam sections (a₁×a₂×t₁×t₂) [mm]	r/c core outer wall thickness [mm]	r/c core inner wall thickness [mm]
1st (ground)	5.0	700×40	700×400×36×20	400	150
2nd - 7th	3.2	700×40	700×400×36×20	400	150
8th - 14th	3.2	650×36	650×360×32×20	350	150
15th - 21st	3.2	600×32	600×320×28×20	300	150
22nd -28th	3.2	550×28	550×280×24×20	250	150
29th- 34th	3.2	500×24	500×240×20×20	200	150
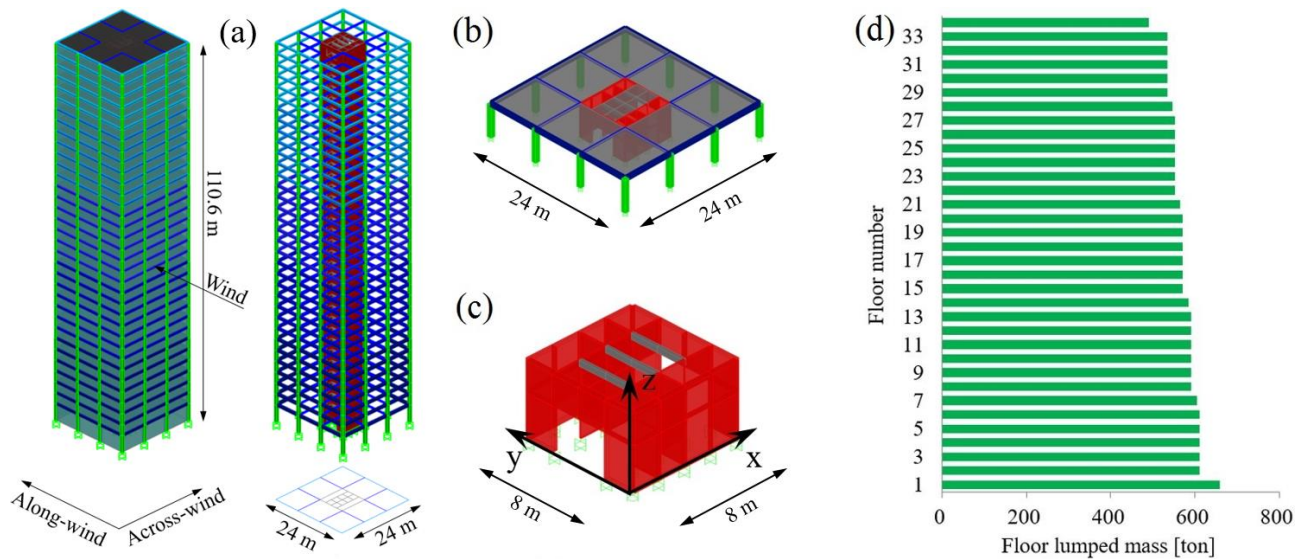
Fig. 2 (a) Case-study 34-storey building; (b) typical floor and core-frame lateral load-resisting system; (c) geometry of r/c core; (d) floor mass distribution.

A linear finite element (FE) model of the building is developed in SAP2000® software package. The FE model comprises 552 membrane and 1564 shell elements, representing the slabs and r/c shear walls, respectively, as well as 1292 Euler-Bernoulli one-dimensional beam elements with rigid or hinged

connections as appropriate. Horizontal perfectly rigid diaphragm constraints are imposed at the height of each floor. The total mass of the structure accounting for dead and live loads is 92830tons and is lumped at each floor level following the distribution shown in Fig.2(d).

Due to the presence of the two large door openings in the r/c core shown in Fig. 2(c), the lateral-load resisting system of the case-study building is not doubly-symmetric in plan. It is found that for the particular wind excitation model adopted in all the ensuing numerical work and discussed later in the paper, the critical (along-) wind field direction is along the y principal building axis inducing maximum lateral floor accelerations along the x principal building axis. Hence, only the in-plane translational vibration motion of the FE model along the x principal axis is required for studying structural performance for occupants' comfort serviceability limit state associated with floor response acceleration in the across-wind direction. To this end, in the next section, a low-order linear planar dynamical model is developed capturing faithfully in-plane structural response to dynamic excitation along x axis of the case-study building in Fig.2.

LOW-ORDER PLANAR MODEL OF UNCONTROLLED CASE-STUDY STRUCTURE

To expedite computational work in later sections, herein, a low-order lumped-mass planar dynamic model with 34 degrees of freedom (DOFs) corresponding to the uncoupled lateral in-plane translations of rigid slabs along the x axis of the case-study building in Fig.2 is derived from the previously discussed detailed FE model. The reasons for using such a relatively large number of DOFs in the low-order model (i.e., one DOF per floor) is to capture accurately the effect of local changes, such as top-storey softening, to the global structural response of the building in support of optimal design and assessment of TMDI-equipped case-study structure as well as to facilitate a fine spatial discretization of the wind loading.

The 34-DOF model is defined in terms of a diagonal mass matrix, $\mathbf{M}_s \in \mathbb{R}^{34 \times 34}$, and full damping and stiffness matrices, $\mathbf{C}_s \in \mathbb{R}^{34 \times 34}$ and $\mathbf{K}_s \in \mathbb{R}^{34 \times 34}$, respectively. Main diagonal of the $\mathbf{M}_s$ matrix is populated with the lumped floor masses in Fig. 2(d) while $\mathbf{K}_s$ and $\mathbf{C}_s$ matrices are obtained as detailed in the following two sub-sections.

Stiffness matrix derivation and verification based on modal properties

The lateral stiffness of the case-study building in Fig.2 along principal axis x is primarily contributed by two planar perimetric three-bay rigid-jointed MRFs and by the r/c core acting along its "weak" axis due to the two openings (i.e., the contribution of the two out-of-plane MRFs is neglected). The MRFs and the core undergo the same lateral displacement at each floor being coupled through rigid diaphragms. In this setting, the coupled core-frame system is modelled as a sum of two contributing cantilevered beam-like structural systems: one corresponding to the r/c core and one to the two same steel MRFs (e.g., Dym and Williams 2007; Cluni et al. 2013). The r/c core contribution is represented by a $\mathbf{K}_{core} \in \mathbb{R}^{34 \times 34}$ stiffness matrix derived from application of static condensation to a flexural

Timoshenko beam as seen in Fig. 3(a). Further, each perimetric MRF is represented by a $\mathbf{K}_{frame} \in \mathbb{R}^{34 \times 34}$ stiffness matrix of an equivalent beam-like structure derived through static condensation as shown in Fig. 3(b). The stiffness matrix of the 34-DOF low-order model can thus be determined as

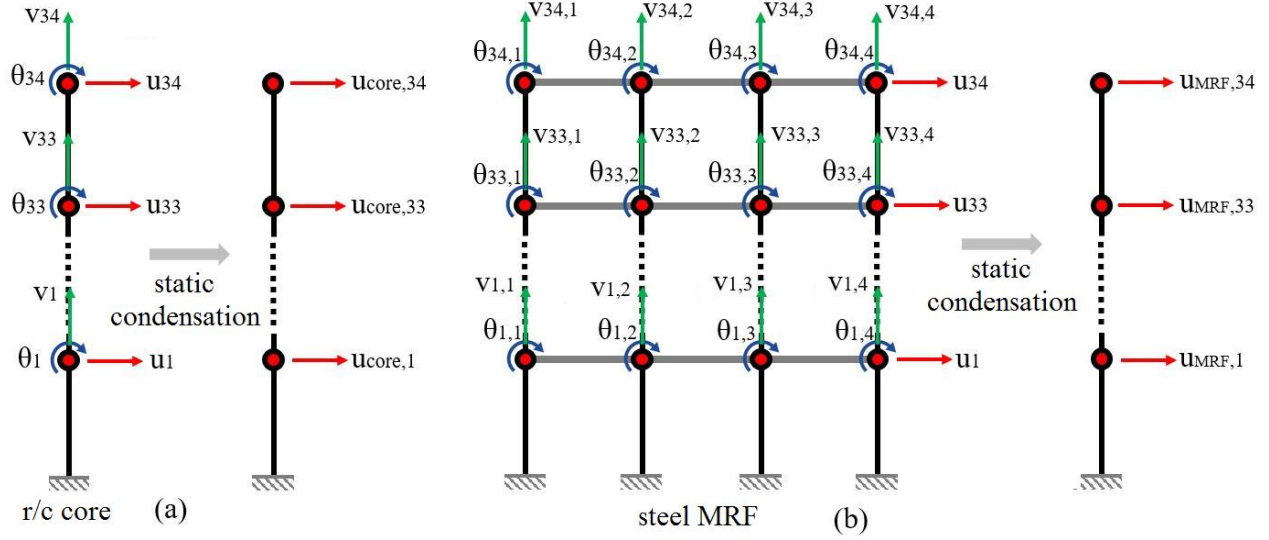$$\mathbf{K}_s = \mathbf{K}_{core} + 2\mathbf{K}_{frame}. \tag{1}$$

Fig. 3. Static condensation for stiffness matrix derivation of the low-order model: (a) for the central core, (b) for the perimetric frame.

The properties of the uncondensed Timoshenko beam in Fig. 3(a) corresponding to the r/c core component are evaluated storey-wise. Effective shear area, cross-sectional area, and second moment of area of the core is determined by accounting for all inner and outer walls along the x principal building axis considering also properties reductions due to door openings. Moreover, the uncondensed stiffness matrix of the 3-bay 34-storey MRF in Fig. 3(b) is determined based on standard FE discretization with Euler-Bernoulli beam elements using columns and beam member sections in Table 1. Importantly, the above approach for $\mathbf{K}_s$ matrix specification allows for modifications to be made independently in any of the two contributing components to the lateral load resisting system (i.e., the MRFs and the r/c core), which facilitates pertinent parametric investigations to be undertaken to explore the performance of TMDI-equipped benchmark structure for different host structure configurations in the numerical part of this work.

The accuracy of the developed 34-DOF low-order model to capture faithfully dynamic modal properties of the detailed FE model of the case-study building even for large local stiffness variations, as will be required in implementing top-storey softening in later sections, is herein verified in terms of natural frequencies and mode shapes for two different r/c core configurations. In the first configuration (baseline uncontrolled structure) the core runs up to the roof (34th floor). In the second configuration,

the core stops at the penultimate storey (33rd floor), thus creating a coreless (flexible) top-storey. The latter configuration is readily implemented in the developed coupled two-beam stiffness matrix derivation approach by setting cross-sectional area and the second moment of area properties of the last segment of the Timoshenko beam in Fig. 3(a) to zero. For both configurations, standard modal analysis is applied to the detailed FE model (Fig. 2) and to the low-order model to extract modal properties corresponding to the translational vibration modes along the x principal axis.

Table 2 reports differences of the lowest three vibration modes obtained from the FE model and the low-order model in terms of natural frequencies and mode shapes. Mode shape difference is quantified through the modal assurance criterion (MAC$_j$) for the *j*-th mode which is a scalar measure of mode shape similarity defined as (Brincker and Ventura 2015)

$$\mathrm{MAC}_j = \frac{\phi_{jlow\_order}^T \phi_{jFEM}}{\left\| \phi_{jlow\_order} \right\| \left\| \phi_{jFEM} \right\|} \qquad (2)$$

where ϕ_{jlow_order} and ϕ_{jFEM} are the *j*-th mode shape vectors obtained by the low-order and the detailed FE model, respectively, the superscript "*T*" denotes matrix transposition and $\| \mathbf{p} \|$ is the length of vector **p**. Clearly, MAC$_j$ value equal to unity means that ϕ_{jlow_order} and ϕ_{jFEM} mode shape vectors are identical. It is seen in Table 2 that, for both configurations, natural frequencies estimated by the low-order model are slightly lower than those computed from the FE model. This is because the contribution of the two out-of-plane MRFs are neglected in the lower-order model. Still, percentage error difference in natural frequencies is below 2% across the board, while MAC values indicate perfect agreement between mode shapes obtained by the two different models. This is further verified visually in Fig.4 which plots the lowest three modes of the two building configurations obtained by the two computational models vis-à-vis.

Table 2. Comparison of modal properties of the lowest 3 translational vibration modes along principal axis y of the case-study building between the detailed FE model and the low-order model

| Core configuration		Mode	Frequency [Hz]			MAC	Mass participation factor
			FEM	Low-order	Error		
Core runs up to 34th floor (baseline uncontrolled structure)		1st	0.3409	0.3344	1.91%	1.000000	63.18%
		2nd	1.3745	1.3537	1.51%	0.999997	18.77%
		3rd	3.2010	3.1651	1.12%	0.999929	7.51%
Core runs up to 33rd floor (coreless top-storey structure)		1st	0.3398	0.3336	1.83%	0.999999	63.19%
		2nd	1.3300	1.3140	1.20%	0.999771	18.82%
		3rd	2.0979	2.0801	0.85%	0.999391	7.27%
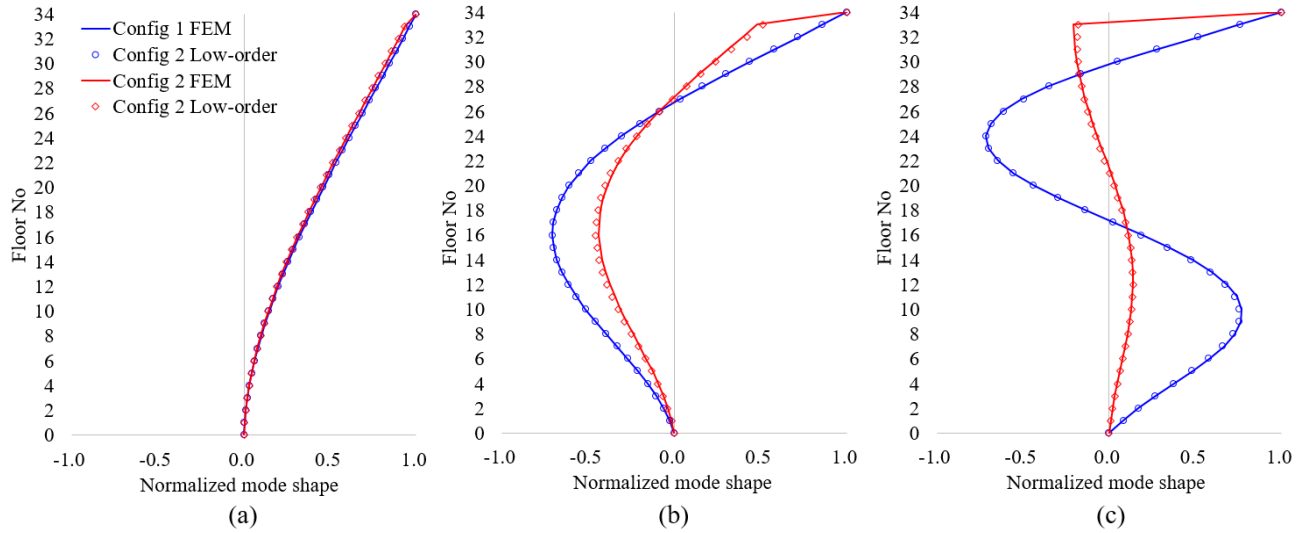
Fig. 4. Lowest three lateral mode shapes for the two different case-study building r/c core configurations of Table 2 obtained by the detailed FE and low-order model: (a) 1st mode, (b) 2nd mode, and (c) 3rd mode.

Overall, matching quality of modal properties quantified in Table 2 and Fig. 4 verify that the herein derived 34-DOF low-order model is dynamically equivalent to the detailed FE model along the x principal direction and will be used henceforth to expedite numerical work.

Inherent damping modelling

The inherent structural damping of the case-study building is incorporated in the low-order model through a full damping matrix obtained by the expression (e.g., Chopra 2000)

$$\mathbf{C_s} = \left(\mathbf{\Phi}^T\right)^{-1}\mathbf{C}_{\text{mod}}\left(\mathbf{\Phi}\right)^{-1} \tag{3}$$

where $\mathbf{\Phi} \in \mathbb{R}^{34\times34}$ is the modal matrix collecting all $\phi_{j\,low\_order}$, j=1,2,…,34 mode shapes, the superscript "-1" denotes matrix inversion, and $\mathbf{C}_{\text{mod}} \in \mathbb{R}^{34\times34}$ is a diagonal matrix defined as

$$C_{\text{mod}}\left[j,j\right] = 2\omega_{n(j)}\xi_j\left(\phi_{j\,low\_order}{}^T\mathbf{M_s}\phi_{j\,low\_order}\right) \quad ; \quad j = 1,2,...,34 \tag{4}$$

In the last equation, $\omega_{n(j)}$ and ξ_j are the j-th natural circular frequency and modal damping ratio, respectively, of the 34-DOF low-order model. In all the ensuing numerical work, unless otherwise specified, the modal damping ratio of the first mode, ξ_1, which dominates the across-wind response of the case-study building, is taken equal to 0.55%. This modal damping ratio value was estimated from field measurements for a similar to the herein considered case-study structure 120m-tall composite building with square floorplan studied in Fang et al. (1997). For higher vibration modes, gradually increasing modal damping ratios are assumed as follows ξ_j= 1% for j = 2,3,4; ξ_j = 2% for j = 5,6,7; ξ_j = 4% for j = 8,9,10; ξ_j = 8% for j = 11,...,20; and ξ_j = 16% for j = 21,...,34, following trends of frequency-dependent damping models for tall buildings proposed in the literature (see e.g., Spence and Kareem 2014 and references therein).

WIND EXCITATION MODEL

Wind action to the low-order 34-DOF planar model derived in the previous section is represented by the stochastic across-wind force model developed by Liang et al. (2002) for tall buildings with rectangular footprint. This wind force model is based on experimental data from a comprehensive wind tunnel testing campaign and accounts for both the turbulent and the VS components of the across-wind force. It is defined by a zero-mean Gaussian ergodic spatially correlated random field expressed in frequency domain through an analytically defined power spectral density (PSD) matrix. Upon spatial discretization of the wind force random field at each floor slab of the case-study 34-storey building, a PSD $\mathbf{S}_{\mathbf{FF}}^{\mathbf{34}} \in \mathbb{R}^{34 \times 34}$ wind force matrix is specified. For the case-study building with total height 110.6m and square footprint the diagonal elements of the PSD wind force matrix, are given as (Liang et al., 2002)

$$S_{FF}^{34}[k,k] = \frac{\sigma_k^2}{\omega}\left[\frac{0.1143\left(\omega/\omega_k\right)^2}{\left(1-\left(\omega/\omega_k\right)^2\right)^2 + 0.041\left(\omega/\omega_k\right)^2} + \frac{0.1633\left(\omega/\omega_k\right)^3}{\left(1-\left(\omega/\omega_k\right)^2\right)^2 + 2\left(\omega/\omega_k\right)^2}\right], k = 1,2,...,34 \quad (5)$$

which specify the PSD of the wind force acting at the k-th floor slab located at height z_k from the ground. In the previous expression, σ_k is the root mean square (RMS) of the across wind force at the k-th floor slab and ω_k is the frequency of VS at z_k height. The RMS of the across wind force is herein computed as

$$\sigma_k = \frac{1}{2}\rho V_m^2(z_k)\bar{C}_L B\Delta z_k , \qquad (6)$$

where ρ is the air mass density taken equal to 1.25kg/m³, $\bar{C}_L$ is the mean RMS lift coefficient which is equal to 0.404 for square footprint buildings according to Liang et al. (2002), B= 24m is the width of the building in the across-wind direction, Δz_k is the tributary height of the k-th floor taken as half the storey height above floor k plus half the storey height below floor k, and $V_m(z_k)$ is the mean wind velocity at z_k height. The latter is determined by (CEN 2005)

$$v_m(z) = c_r(z)c_o(z)v_b , \qquad (7)$$

where v_b is the basic wind velocity (i.e., the 10 minute mean wind velocity at 10m above open flat country terrain) taken equal to 22 m/s throughout this work, $c_o(z)$ is the orography factor assumed equal to 1.0, and $c_r(z)$ is the roughness factor based on the Eurocode-compliant logarithmic law and terrain category IV (i.e., area in which at least 15% of the surface is covered with buildings and their average height exceeds 15 m). Further, the VS frequency is determined by

$$\omega_k = \frac{2\pi S_t v_m\left(z_k\right)}{B} , \qquad (8)$$

in which S_t is the Strouhal number taken equal to 0.084 as experimentally determined by Liang et al. (2002) for square footprint tall buildings.

For illustration, the PSDs of wind force acting at four different floor slab heights are plotted in Fig. 5 for $v_b = 22$ m/s. It is seen that the dominant VS frequency increases with floor height as can be inferred by Eqs. (7) and (8). The same happens for the wind force amplitude except from the last floor whose tributary height is different from the rest of the building floors, i.e., 1.6 m as opposed to 3.2 m applicable for the typical floor.
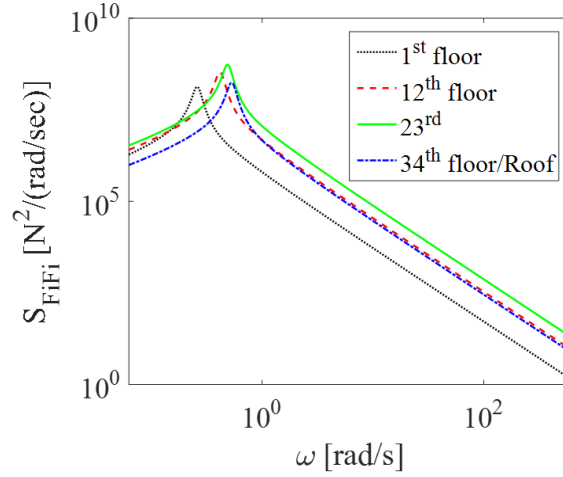

Fig. 5. Power spectral density functions of across-wind forces acting at different floor levels of the case-study building.

The off-diagonal terms of the $\mathbf{S_{FF}^{34}}$ PSD matrix modelling the spatial correlation of wind forces acting at floor slabs k and l are given as (Liang et al., 2002)

$$S_{FF}^{34}[k,l] = \exp\left[-\left(\frac{z_k - z_l}{133.44}\right)^2\right]\sqrt{S_k(\omega)S_l(\omega)}, \tag{9}$$

for the case-study building.

MODELLING AND ANALYSIS OF TMDI-EQUIPED CASE-STUDY BUILDING IN ACROSS-WIND DIRECTION

The TMDI is a linear passive dynamic vibration absorber introduced by Marian and Giaralis (2013, 2014) for supressing the lateral motion of seismically excited multi-storey building structures amenable to modelling as planar MDOF systems with mass properties lumped at each floor. As discussed in the introduction (Fig. 1), the potential of a top-storey TMDI is examined to mitigate wind-induced floor accelerations in the across-wind direction of the case-study structure with a softened top-floor. This section discusses the modifications required to incorporate a top-storey TMDI to the low-order 34-DOF model of the case-study building as well as a computationally efficient frequency domain analysis approach to determine the response of TMDI-equipped low-order building model to the across-wind excitation presented in the previous section.

TMDI incorporation to the low-order case-study building model

Suppose that the 34-DOF low-order model of the case-study building is visualised as a 34-storey coupled MRF-shear wall planar structure with lumped floor masses $m_k = M_s[k,k]$, $k=1,2,\ldots,34$ as shown in Fig.1(a) for $n=34$. Then, a top-storey TMDI (topology "-1") can be readily incorporated to the low-order model as graphically shown in Fig. 1(d). Specifically, the TMDI consists of a conventional TMD comprising a secondary m_{TMDI} mass attached to the top (34th) floor via a stiffener, modelled as a linear spring with k_{TMDI} stiffness, in parallel with a linear viscous damper, modelled as a dashpot with damping coefficient c_{TMDI}, and an inerter device, highlighted in red in Fig. 1(d), connecting the secondary mass to the penultimate (33rd) floor. The inerter device is modelled through an ideal massless mechanical element resisting the relative acceleration developing at its two ends through the inertance coefficient b (Smith 2002). Under the above assumptions, the mass, $\mathbf{M} \in \mathbb{R}^{35\times35}$, the damping, $\mathbf{C} \in \mathbb{R}^{35\times35}$, and the stiffness, $\mathbf{K} \in \mathbb{R}^{35\times35}$, matrices of the TMDI-equipped low-order 34-DOF model can be written as

$$
\mathbf{M} = \begin{bmatrix} m_1 & 0 & \cdots & \cdots & \cdots & 0 \\ 0 & m_2 & \cdots & \cdots & \cdots & \vdots \\ \vdots & \vdots & \ddots & 0 & 0 & 0 \\ \vdots & \vdots & 0 & m_{33}+b & 0 & -b \\ \vdots & \vdots & 0 & 0 & m_{34} & 0 \\ 0 & \cdots & 0 & -b & 0 & m_{TMDI}+b \end{bmatrix}, \quad
\mathbf{C} = \begin{bmatrix} c_{1,1} & c_{1,2} & \cdots & \cdots & c_{1,34} & 0 \\ & c_{2,2} & \cdots & \cdots & \vdots & \vdots \\ & & \ddots & c_{32,33} & c_{32,34} & 0 \\ & & & c_{33,33} & c_{33,34} & 0 \\ & SYM & & & c_{34,34}+c_{TMDI} & -c_{TMDI} \\ & & & & & c_{TMDI} \end{bmatrix},
$$

$$
\text{and} \quad \mathbf{K} = \begin{bmatrix} k_{1,1} & k_{1,2} & \cdots & \cdots & k_{1,34} & 0 \\ & k_{2,2} & \cdots & \cdots & \vdots & \vdots \\ & & \ddots & k_{32,33} & k_{32,34} & 0 \\ & & & k_{n-1,n-1} & k_{33,34} & 0 \\ & SYM & & & k_{34,34}+k_{TMDI} & -k_{TMDI} \\ & & & & & k_{TMDI} \end{bmatrix},
$$

(10)

in which $k_{k,l} = K_s[k,l]$ and $c_{k,l} = C_s[k,l]$ where $k,l=1,2,\ldots,34$ are the elements of the matrices defined in Eqs. (1) and (3), respectively, while the 35-th DOF corresponds to the lateral TMDI mass displacement. Note that the inclusion of the inerter device influences only the mass matrix $\mathbf{M}$ (i.e. the matrices $\mathbf{C}$ and $\mathbf{K}$ are the same for the TMD and for the TMDI), which is non-diagonal as the inerter couples the motion of the secondary mass and the penultimate floor in terms of *accelerations* only. Further, note that for $b=0$ the mass matrix of a 34-storey lumped-mass core-frame building with a TMD attached to the top floor is retrieved (i.e. the TMD is a special case of the TMDI). For $b\neq0$, the inerter element force developed in the dynamical system reads as (see also Smith 2002)

$$
F_b = b(\ddot{x}_{TMDI} - \ddot{x}_{33}), \tag{11}
$$

where x_{TMDI} is the lateral displacement of the secondary mass, x_{33} is the lateral displacement of the penultimate building floor and a dot over a symbol signifies differentiation with respect to time. Therefore, in the TMDI configuration the inerter exerts an additional, compared to the conventional

TMD, force, F_b, to the host structure whose amplitude depends on the relative acceleration between the secondary mass and penultimate floor and on the inertance b. The latter factor depends on the inerter device specifications and can reach very large values of the order of 10^3 tons as extensively discussed in the literature (e.g. Smith 2002, Nakaminami et al. 2016, Giaralis and Petrini 2017). The potentially beneficial influence of the inerter to the performance of the TMDI-equipped structure is parametrically examined in the numerical part of this paper through optimal TMDI design/tuning and structural performance assessment to wind excitation for different inertance values and top-storey lateral stiffness. Structural analysis of the TMDI-equipped low-order model to wind excitation required for both optimal TMDI design and performance assessment is undertaken using the following frequency domain approach.

Frequency domain analysis for the TMDI-equipped structure under wind excitation

The response displacement, velocity and acceleration PSD matrices of the TMDI-equipped low-order model defined by the **M**, **C**, and **K** matrices in Eq. (10) due to the $\mathbf{S}_{FF}^{34}$ matrix can be obtained using the frequency domain input-output relationships of random vibrations (e.g. Soong and Grigoriu 1993) as in

$$\mathbf{S}_{\mathbf{xx}}(\omega) = \mathbf{B}(\omega)^* \mathbf{S}_{\mathbf{FF}}(\omega)\mathbf{B}(\omega), \quad \mathbf{S}_{\ddot{\mathbf{x}}\ddot{\mathbf{x}}}(\omega) = \omega^2 \mathbf{S}_{\mathbf{xx}}(\omega), \text{ and } \quad \mathbf{S}_{\ddot{\mathbf{x}}\ddot{\mathbf{x}}}(\omega) = \omega^4 \mathbf{S}_{\mathbf{xx}}(\omega), \tag{12}$$

respectively. In Eq. (12), $\mathbf{S}_{FF}$ is the PSD wind force matrix $\mathbf{S}_{FF}^{34}$ augmented by a zero bottom row and a zero rightmost column corresponding to the TMDI lateral mass displacement which is not subjected to any wind load being internally housed. Further, the "*" superscript denotes complex matrix conjugation, and the transfer matrix **B** is given as

$$\mathbf{B}(\omega) = \left(\mathbf{K} - \omega^2 \mathbf{M} + i\omega \mathbf{C}\right)^{-1}, \tag{13}$$

where, $i = \sqrt{-1}$. Next, response acceleration variance of the k-th floor is obtained as

$$\sigma_{\ddot{x}_k}^2 = \int_0^{\omega_{max}} S_{\ddot{x}_k \ddot{x}_k}(\omega) d\omega, \tag{14}$$

that is, by integrating the response auto-spectra populating the main diagonal elements of the response acceleration PSD matrix in Eq. (12) on the frequency axis up to a maximum (cut-off) frequency ω_{max} above which the energy of the underlying processes is negligible. Moreover, the variance of the relative response displacement, velocity, and acceleration between floors/DOFs k and l are obtained by (e.g. Soong and Grigoriu 1993)

$$\sigma^2_{x_{kl}} = \sigma^2_{x_k} + \sigma^2_{x_l} - 2 \int_0^{\omega_{max}} S_{x_k x_l}(\omega) d\omega,$$

$$\sigma^2_{\dot{x}_{kl}} = \sigma^2_{\dot{x}_k} + \sigma^2_{\dot{x}_l} - 2 \int_0^{\omega_{max}} S_{\dot{x}_k \dot{x}_l}(\omega) d\omega, \text{ and} \qquad (15)$$

$$\sigma^2_{\ddot{x}_{kl}} = \sigma^2_{\ddot{x}_k} + \sigma^2_{\ddot{x}_l} - 2 \int_0^{\omega_{max}} S_{\ddot{x}_k \ddot{x}_l}(\omega) d\omega,$$

where $S_{x_k x_l}(\omega) = S_{xx}[k,l]$, $S_{\dot{x}_k \dot{x}_l}(\omega) = S_{\dot{x}\dot{x}}[k,l]$, and $S_{\ddot{x}_k \ddot{x}_l}(\omega) = S_{\ddot{x}\ddot{x}}[k,l]$ are the response displacement, velocity, and acceleration cross-spectra corresponding to the k and l DOFs. Ultimately, the peak acceleration of the k-th floor can be estimated by the expression

$$\text{peak}\{\ddot{x}_k\} = g\sqrt{\sigma^2_{\ddot{x}_k}}, \qquad (16)$$

while and the peak relative displacement, velocity, and acceleration between k and l DOFs, are estimated by

$$\text{peak}\{x_{kl}\} = g\sqrt{\sigma^2_{x_{kl}}}, \quad \text{peak}\{\dot{x}_{kl}\} = g\sqrt{\sigma^2_{\dot{x}_{kl}}}, \text{and} \quad \text{peak}\{\ddot{x}_{kl}\} = g\sqrt{\sigma^2_{\ddot{x}_{kl}}}, \qquad (17)$$

respectively. In Eqs. (16) and (17), g is the peak factor estimated by the widely used empirical formula due to Davenport (1964)

$$g = \sqrt{2ln(\eta T_{wind})} + \frac{0.577}{\sqrt{2ln(\eta T_{wind})}}, \qquad (18)$$

where $\eta = 2\pi/\omega_{n(1)}$ and T_{wind} is the time duration of exposure to the wind action during which the peak response quantities in Eqs.(16) and (17) are attained under the assumption of input/output stochastic processes being stationary/ergodic time-limited processes. In all the ensuing numerical work, T_{wind} is taken equal to 3600s (i.e., one hour of stationary wind excitation is assumed).

OPTIMAL TMDI DESIGN FOR SERVICEABILITY PERFORMANCE ACCOUNTING FOR TOP-STOREY STIFFNESS REDUCTION

To investigate the potential of top-storey softening for enhanced serviceability performance in TMDI-equipped wind-excited tall buildings subject to VS effects, it is deemed essential to optimally tune the TMDI to minimize peak floor accelerations for pre-specified wind excitation and building structure properties. This is because peak floor acceleration is the critical response quantity in meeting serviceability limit state criteria associated with occupants' motion perception (Kwok et al. 2009). To this aim, a novel optimal TMDI tuning problem is herein formulated and applied to the case-study structure in which top-storey stiffness is explicitly accounted for in the design. The presentation begins with the optimal design problem formulation, followed by discussion on the numerical solutions strategy, optimality achieved, and robustness of optimal TMDI properties to top-storey stiffness in view

of selective numerical results.

Optimal design problem formulation

The proposed optimal TMDI tuning for *n*-storey buildings with softened top-storey aims to minimize the peak acceleration of the *n*-2 floor. This minimization criterion is adopted since floor acceleration increases monotonically with building height in typical structures while it is assumed that, upon TMDI installation and structural modifications (softening) at the top-storey, the penultimate is the highest occupied storey (Fig.1). The considered optimization problem involves 5 design parameters, namely the TMDI frequency and damping ratios defined as

$$\upsilon_{TMDI} = \frac{\sqrt{\dfrac{k_{TMDI}}{(m_{TMDI}+b)}}}{\omega_{n(1)}} \quad \text{and} \quad \xi_{TMDI} = \frac{c_{TMDI}}{2\sqrt{(m_{TMDI}+b)k_{TMDI}}}, \tag{19}$$

respectively, and grouped in the vector $\mathbf{y_1}=[\upsilon_{TMDI} \quad \xi_{TMDI}]^T$, as well as the top-storey height, H_{top}, and the TMDI mass and inertance ratios defined as

$$\mu = \frac{m_{TMDI}}{M_{tot}} \quad \text{and} \quad \beta = \frac{b}{M_{tot}}, \tag{20}$$

respectively, where M_{tot} is the total building mass, grouped in the vector $\mathbf{y_2}=[H_{top} \quad \mu \quad \beta]^T$. The optimization problem involves determining optimal design parameters in $\mathbf{y_1}$ (primary design variables) within a pre-specified search range $[\mathbf{y_1^{min}}, \mathbf{y_1^{max}}]$ that minimize the objective function (OF), $\text{peak}\{\ddot{x}_{n-2}\}$, given values of the parameters in $\mathbf{y_2}$ (secondary design parameters). The problem can be mathematically expressed as

$$\min_{\mathbf{y_1}}\left[\text{OF}(\mathbf{y_1}|\mathbf{y_2})\right], \quad \text{where} \quad \text{OF=peak}\{\ddot{x}_{n-2}\}, \quad \text{subjected to} \quad \mathbf{y_1^{min}} \le \mathbf{y_1} \le \mathbf{y_1^{max}}. \tag{21}$$

For the adopted case-study building the objective function is $\text{OF=peak}\{\ddot{x}_{32}\}$ computed by Eq. (16).

Purposely, the above optimal design formulation allows for considering explicitly any desired combination of TMDI inertial properties, that is, attached mass and inertance, through the secondary design parameters μ and β, respectively. In this manner, the special case of the TMD ($\beta=0$) can be examined. Furthermore, the formulation utilizes a single geometric property, top-storey height, to leverage the level of top-storey softening or, equivalently, of top-storey lateral stiffness reduction in a straightforward manner whilst, in an actual application, top-storey stiffness reduction may be implemented by one, or a combination of, several other local (top-storey) structural modifications apart from discontinuing the r/c core. These may include the reduction of flexural rigidity of beams and/or columns of the MRF and the increase of top-storey height. More importantly, the reason of including a host/building structure parameter to TMDI design is because the lateral stiffness of the top-storey

(where the TMDI is installed) influences heavily TMDI (though not TMD) optimal primary design parameters as will be seen in view of numerical results.

Numerical solution strategy and nature of achieved optimality

The optimization problem in Eq. (21) is numerically solved for the case-study structure using a pattern search algorithm (Charles and Dennis, 2003) with iteratively updated search range of the primary variables hard-coded in MATLAB®. A wide *initial* search range delimited by $\mathbf{y_1^{min}} = [0.0,\ 0.0]^T$ and $\mathbf{y_1^{max}} = [2.0,\ 2.0]^T$ is adopted since it is found that optimal TMDI tuning parameters move away from the commonly encountered values for building structures with smooth stiffness variation in elevation as top-storey stiffness reduces (e.g., optimal frequency ratios υ_{TMDI} are much higher than unity corresponding to tuning to the first mode of the uncontrolled structure as seen later in Fig. 7). To expedite computations in solving Eq. (21), the custom-developed algorithm applies pattern search iteratively with progressively narrower search range in $\mathbf{y_1}$ by "zooming-in" the neighborhood of the optimal υ_{TMDI} and ξ_{TMDI} values found in the previous iteration. The stoppage criterion for the iterations checks the absolute difference between two successive optimal OF values against a pre-specified convergence tolerance.
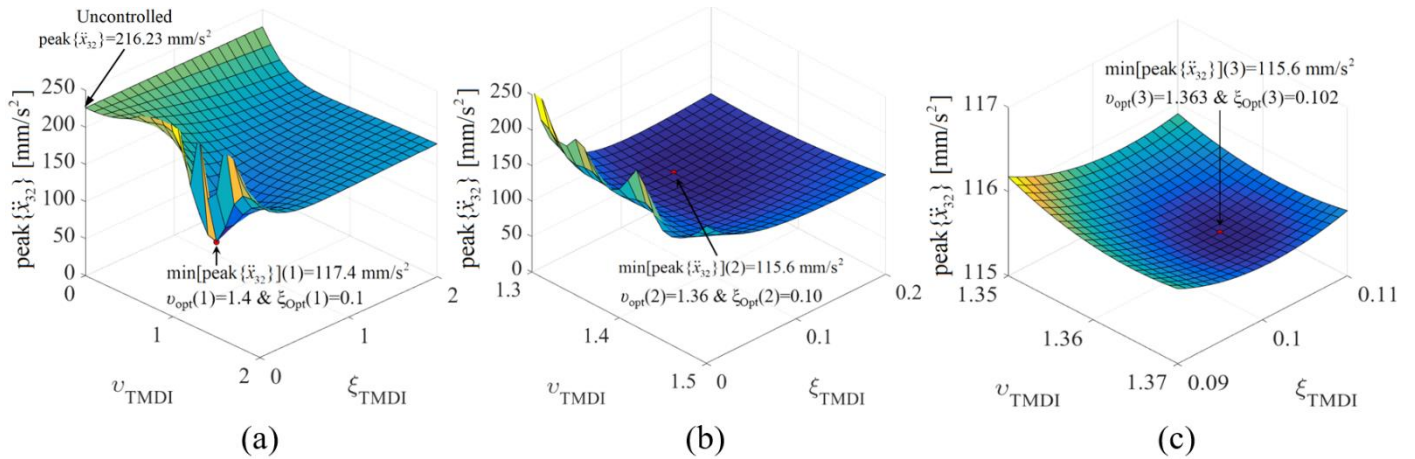

Fig. 6 Iterative optimal TMDI design with μ=0.1% and β=8% for the adopted case-study structure with H_{top}=5m and discontinued r/c core (a) 1st iteration, (b) 2nd iteration, and (c) 3rd iteration.

For numerical illustration, Fig. 6 plots OF surfaces on the primary design variable plane (υ_{TMDI}, ζ_{TMDI}) obtained from the iterative pattern search-based algorithm for the case-study structure with coreless top-storey for $\mathbf{y_2}$=[H_{top}=5m, μ=0.1%, β=8%]^T and for the wind excitation PSD $\mathbf{S_{FF}}$. The global minimum point $\left(\upsilon_{opt}(p), \xi_{opt}(p), peak\{\ddot{x}_{32}\}(p)\right)$ for the p-th iteration is further reported in Fig. 6. The convergence tolerance is set to 1 mm/s^2. For this case, convergence is reached after three iterations in which the initial search range narrows down to $\mathbf{y_1^{min}} = [1.3,\ 0.0]^T$ and $\mathbf{y_1^{max}} = [1.5,\ 0.2]^T$ in the second iteration, and ultimately to $\mathbf{y_1^{min}} = [1.35,\ 0.09]^T$ and $\mathbf{y_1^{max}} = [1.37,\ 0.11]^T$ in the final iteration, with same discretization of the search domain and with logarithmic increase of precision/resolution by which optimal parameters are determined.

To shed light on the nature of optimality achieved through solving Eq.(21) for buildings with flexible top-storey, Fig. 1(e) plots the 32nd floor acceleration frequency response function (FRF) of the optimal TMDI-equipped example structure treated in Fig. 6 (softened top-storey case) together with the FRFs for optimal TMDI-equipped structure with coreless top-storey modification (topology "-1" case) and for uncontrolled/unmodified structure. It is seen that the considered optimal TMDI design formulation yields a classical "Den Hartog" style of optimality (Den Hartog 1947): both FRFs of TMDI controlled structures attain two local resonant peaks of almost equal height one to the left and one to the right of the fundamental natural frequency of the uncontrolled structure $\omega_{n(1)}$. Evidently, this type of optimality *is maintained under the herein considered building modification* (i.e., top-storey softening) since the latter does not change significantly $\omega_{n(1)}$ (see Table 2). Notably, it is known that Den Hartog optimality is mostly efficient for supressing narrow-band excitations characterized by a dominant frequency and, therefore, relevant to addressing VS effects (see Fig.5). Moreover, the higher-natural-frequency (i.e., wideband) damping effect of TMDI, which is well-reported in the literature (Giaralis and Taflanidis 2015, 2018), becomes more prominent with top-storey softening Fig. 1(e): the second resonant peak in the FRF of the uncontrolled structure is slightly reduced in the FRF of TMDI-equipped unmodified structure, while it is practically non-visible in the FRF of the TMDI-equipped structure with top-storey softening.

Sensitivity of optimal primary design parameters to top-storey stiffness

The influence of top-storey stiffness to the optimal TMDI parameters in $\mathbf{y_1}$ determined through solving Eq. (21) is parametrically investigated in Fig.7 considering the cases of TMDI with μ=0.1%, β=6% and structures with coreless top-storey and with different top-storey heights H$_{top}$=4m, 5m, and 6m. All panels of Fig.7 plot the peak$\{\ddot{x}_{32}\}$ of TMDI-controlled structures normalized by peak$\{\ddot{x}_{32}\}$ of the uncontrolled and unmodified case-study building versus the frequency ratio υ_{TMDI} and/or the damping ratio ξ_{TMDI}. It is seen that, as top-storey stiffness reduces (i.e., top-storey height increases), optimal υ_{TMDI} and ξ_{TMDI} values increase appreciably. The fact that ξ_{opt} increases with top-storey softening for fixed TMDI inertial properties (i.e., secondary mass and inertance) is quite welcoming as it has been shown to be well-associated with improved TMDI motion control capacity for seismically excited multi-storey buildings (Ruiz et al. 2018, Taflanidis et al. 2019). This trend is herein confirmed as the minimum achieved peak$\{\ddot{x}_{32}\}$ value attained at the optimal TMDI design point reduces considerably as ξ_{opt} increases driven by higher top-storey building height (last row of panels in Fig.7).

From a structural dynamics viewpoint, it appears that TMDI stiffness is key to the improved TMDI motion control potential as top-storey becomes more flexible. Indeed, υ_{opt} increases significantly with top-storey height (e.g., TMDI frequency becomes 60% higher from the first natural frequency of the uncontrolled structure $\omega_{n(1)}$ for the case of H$_{top}$=6m) demonstrating that TMDI resonates with local top-storey dynamics associated with higher frequencies as the top-storey stiffness reduces (see e.g., mode shapes of uncontrolled case-study building structure with coreless top-storey in Fig.4). Notably, such large υ_{opt} values are not observed in optimal TMDI designs for regular in elevation structures in which υ_{opt} ranges typically within [0.8 1.0] interval (Ruiz et al. 2018) even in the case of TMDI topologies

with inerters spanning more than one storey (e.g., topology "-2" in Fig.1). Even more important, from a practical viewpoint, is to observe in Fig.7 that the optimal TMDI design/tuning becomes significantly less sensitive to the optimal TMDI parameters in $\mathbf{y_1}$ as the top-storey becomes more flexible: perturbations to υ_{opt} and/or ξ_{opt} values have less impact to the achieved peak $\{\ddot{x}_{32}\}$ performance as top-storey height increases. Therefore, top-storey softening increases TMDI robustness to design parameters and, ultimately, to uncertain or inaccurate knowledge of the fundamental natural frequency of the uncontrolled structure as well as to detuning effects which are major concerns in passive TMD applications (Elias and Matsagar 2017).
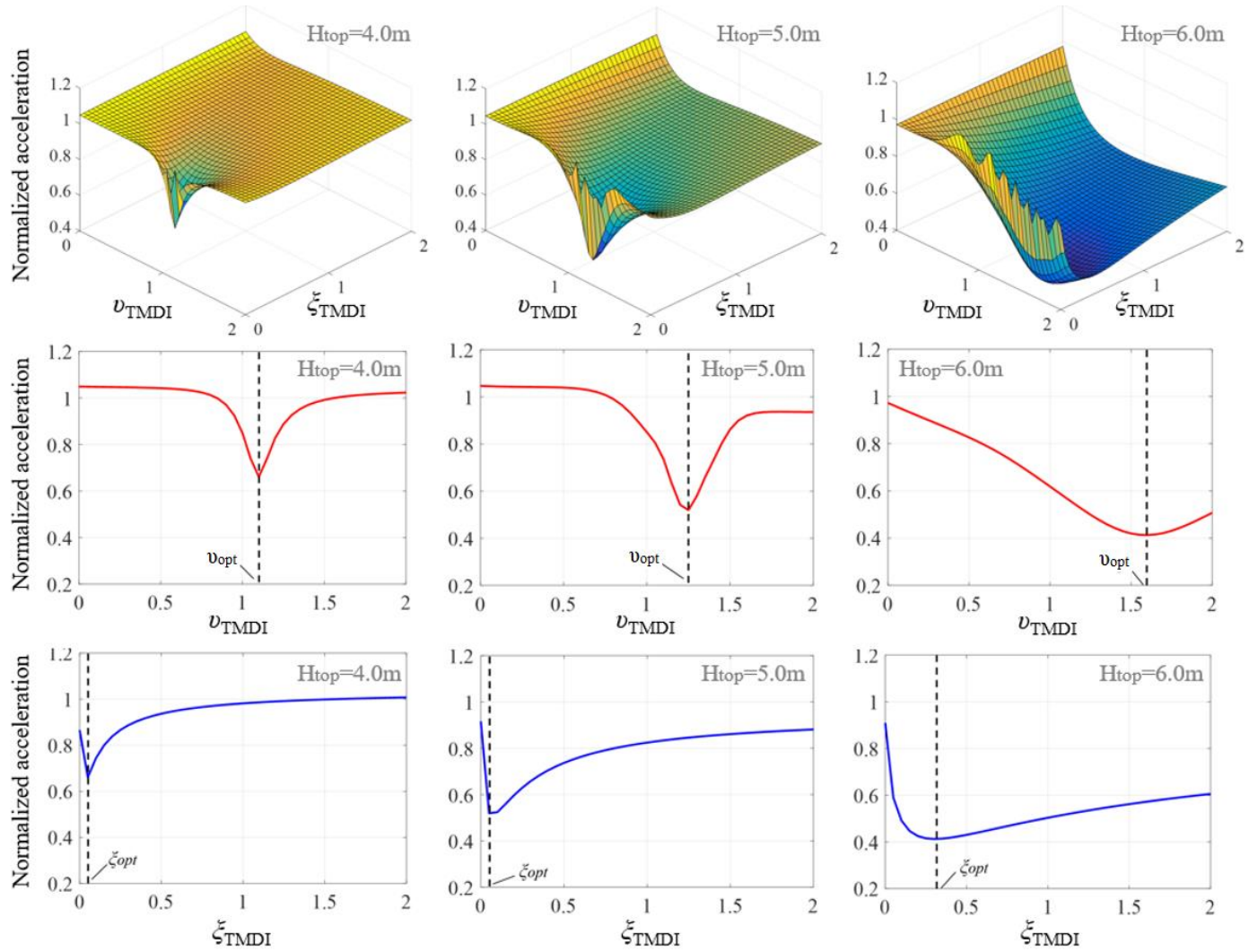

Fig. 7 Objective function surface on the primary design variables plane (upper row of panels) and surface cross-sections along υ_{TMDI} at the optimal $\xi_{TMDI}= \xi_{opt}$ value (middle row of panels), and along ξ_{TMDI} at the optimal $\upsilon_{TMDI}= \upsilon_{opt}$ value (lower row of panels) for μ=0.1%, β=6%, and various top storey heights H$_{top}$.

PERFORMANCE ASSESSMENT AND DESIGN OF OPTIMAL TMDI-EQUIPPED STRUCTURE WITH REDUCED TOP-STOREY STIFFNESS

In this section, comprehensive numerical results are furnished and discussed shedding light to the effectiveness of TMDI designed/tuned through the solution of the optimization problem in Eq.(21) in containing VS induced vibrations in the case-study building exposed to the $\mathbf{S_{FF}^{34}}(\omega)$ PSD wind force matrix. To this aim, TMDIs with different inertial properties (i.e., secondary mass and inertance) are examined while the top-storey of the case-study building is softened laterally by eliminating the r/c core and by varying its height within h= [4.0, 6.0] (m) interval. Firstly, performance in terms of peak floor acceleration of the 32nd floor as well as peak secondary mass stroke (relative displacement between secondary mass and 33rd floor) is presented and discussed. Next, peak developed damping and inerter forces are reported to gain an insight on their relative importance as TMDI properties vary. Lastly, attention is focused on quantifying the trade-offs among secondary mass, inertance and top-storey stiffness to explore the feasibility of more lightweight TMDIs achieving a pre-specified structural performance in terms of peak floor acceleration (i.e., performance-oriented design).

Floor acceleration and secondary mass stroke

The first row of panels in Fig.8 reports percentage reduction factor (RF) of peak floor acceleration at the 32nd floor of optimal TMDI-equipped structure with respect to the uncontrolled case-study building with a coreless (flexible) top-storey (i.e., the core stops at the penultimate/33rd storey) for three different mass ratios and for several inertance ratios including the limiting case of β=0 (TMD) as a function of top-storey lateral stiffness. The latter is given as a percentage of the top-storey stiffness of the case-study structure without r/c core at the 33rd storey and h=3.2m. It is observed that optimal TMDI capability to suppress floor accelerations increases appreciably and monotonically as the top-storey stiffness reduces for fixed mass and inertance ratios (but for different TMDI stiffness and damping properties as determined through the solution of the optimization problem in Eq.(21)). On the antipode, for the TMD case (i.e., no inerter) acceleration RFs remain practically constant with top-storey flexibility. These results demonstrate that the very presence of the inerter (i.e., as long as b>0) enables improved TMDI vibration control potential as top-storey flexibility increases. This fact is attributed to the coupling of the acceleration of the secondary oscillating mass to the acceleration of the 33rd floor achieved by the inerter mathematically manifested through the non-diagonal terms in the mass matrix **M** in Eq.(10). And the herein advocated host-structure modification (i.e., top-storey softening) leverages the positive effect of this coupling in reducing floor accelerations *below the top-storey*. Nevertheless, when no such coupling exists (i.e., conventional TMD case in which β=b=0 and **M** in Eq.(10) is a diagonal matrix), top-storey flexibility has no effect to the overall motion control level achieved. In the latter case, the appended secondary mass does not "see" the local top-storey change of stiffness and, therefore, the TMD is trivially tuned to the first natural frequency of the host structure (note that ν_{opt}=1 across the board in the second row of panels in Fig.8) which remains practically unchanged with top-storey stiffness (see e.g., first natural frequencies for unmodified and top-storey coreless uncontrolled building in Table 2).

In this regard, top-storey lateral stiffness becomes a critical TMDI design parameter (though not for TMD). For example, for TMDI with μ=0.1% and β=8%, a reduction to top-storey stiffness from 53% to 18% (herein implemented by increasing top-storey height h from 4.0m to 5.8m) achieves 20% improvement in reducing peak 32nd floor acceleration *and* 10% better performance compared to the TMD with same attached mass. Moreover, it is seen that for given μ and β there is a limiting top-storey stiffness reduction defined by the intersection of the (practically horizontal) TMD RF curves with the TMDI RF curves, above which the TMD outperforms TMDI. This limiting value increases (i.e., less severe top-storey softening is required for TMDI to outperform TMD) as inertance increases and secondary mass reduces.

Furthermore, for fixed top-storey stiffness, higher inertance improves floor acceleration control at a reduced rate with inertance. This improvement becomes more significant for increased top-storey flexibility and for reduced attached mass, that is, TMDI RF curves are more spaced out as top-storey stiffness reduces and/or μ decreases. Notably, these trends confirm results reported in the literature for the case of a high-rise 74-storey wind-excited building (Petrini et al. 2020) as well as for seismically excited low-to-mid-rise buildings with optimal TMDIs (Giaralis and Taflanidis 2018, Ruiz et al. 2018).
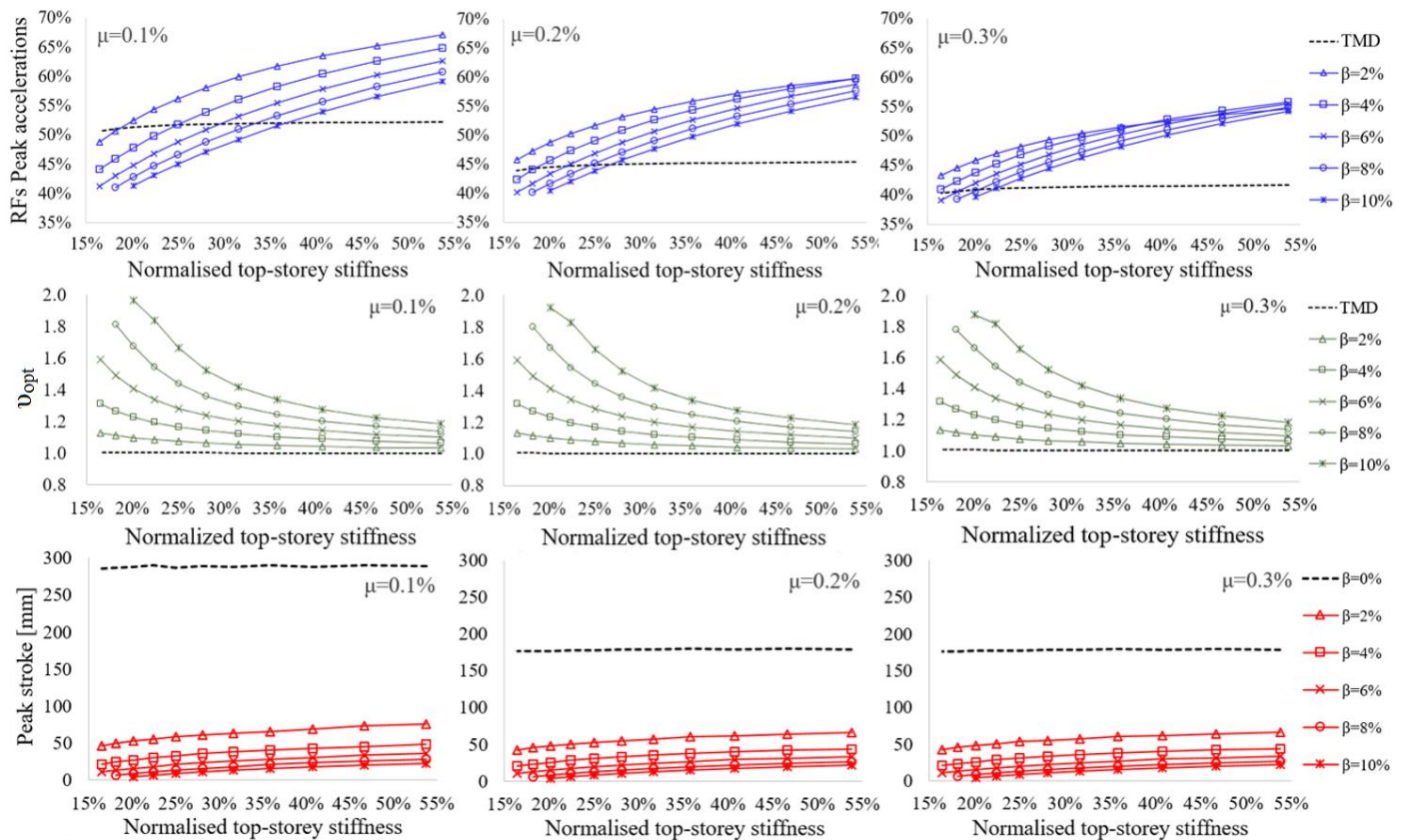

Fig. 8 Peak acceleration percentage reduction of 32nd floor (upper row of panels), optimal frequency ratio (middle row of panels), and secondary mass stroke (lower row of panels), in TMDI-equipped structure for various mass ratios, μ, and inertance ratios, β, against lateral top-storey stiffness reduction.

Apart from peak floor acceleration, which is the critical building performance index for serviceability

limit state design in the across-wind direction, an important quantity of interest to practical design of mass/inertial dampers is the so-called peak stroke of the secondary mass, that is, the peak relative displacement of the TMD(I) mass with respect to the floor that the mass is attached to. This is because increased TMD(I) stroke demands require larger clearance in housing safely a TMDI within the host structure such that no local pounding/collision occurs. Further, the cost of damper device increases with stroke. For the case-study structure, the peak stroke is computed by setting k=34 and l=35 (i.e., DOF corresponding to the secondary mass displacement) in $\text{peak}\{x_{kl}\}$ expression in Eq.(17). The bottom row of panels in Fig. 8 plots peak TMD(I) stroke for the same inertial properties versus top-storey stiffness reduction. It is seen that the inclusion of the inerter reduces considerably secondary mass stroke demands, as also by Giaralis and Petrini (2017) for non-optimally tuned TMDIs, and that peak stroke reduces with increasing inertance at a reduced rate. The gains in stroke demand of the TMDI compared to TMD reduce as secondary mass increases but remain significant (almost 6-fold stroke reduction for μ=0.1 reducing to almost 4-fold reduction for μ=0.2 and 0.3). More importantly, stroke demand is positively (though insignificantly) affected by top-storey stiffness reduction. This is quite welcoming result suggesting that the favourable effect of increasing top-storey flexibility to the TMDI effectiveness for mitigating floor accelerations does not come with any increasing cost/demand related to the stroke of the damping device or to the clearance of the secondary mass.

Inerter force and damping force

To gain further insight to the effect of top-storey stiffness reduction to TMDI motion control capacity, attention is herein focused on quantifying the peak forces developing at the inerter and at the damping device of optimally designed TMDIs according to Eq.(21). The quantification of peak inerter and damping forces is also deemed essential to check that they are not excessive and, thus, can be economically accommodated locally by the host structure as this is found to be critical for TMDIs used in seismic protection of building structures (see e.g., Ruiz et al. 2018 and Taflanidis et al. 2019). In this respect, the upper two rows of panels in Fig. 9 report peak inerter and damping device forces for the same optimal TMDI designs examined in Fig.8. The peak relative acceleration required in determining the peak inerter force in Eq.(11), is computed by setting k=33 and l=35 in $\text{peak}\{\ddot{x}_{kl}\}$ expression in Eq.(17), while the peak damping force is computed by the product of the peak relative velocity between the secondary mass and last floor found by setting k=34 and l=35 in $\text{peak}\{\dot{x}_{kl}\}$ expression in Eq.(17) and the damping coefficient, c_{opt}, determined by

$$c_{opt} = 2\xi_{opt}\upsilon_{opt}(m_{TMDI} + b)\omega_{n(1)}. \qquad (22)$$

The latter expression is obtained by setting υ_{TMDI} and ξ_{TMDI} equal to υ_{opt} and ξ_{opt}, respectively, in Eq.(19) and manipulating. Results evidence that secondary mass has negligible effect to the inerter and damping forces, while these forces increase monotonically with inertance for fixed mass ratio and top-storey stiffness. The effect of the inertance to the inerter force is readily deduced from Eq.(11) and confirms trends reported by Giaralis and Petrini (2017) for non-optimal TMDIs for VS-induced vibrations mitigation in tall buildings. Further, the positive relationship between inertance and damping force, also seen in TMDIs optimized for seismic protection of multi-storey buildings (Ruiz et al. 2018), is attributed

to the fact that c_{opt} in Eq.(22) increases with inertance since ξ_{opt} (reported in the bottom row of panels in Fig. 9) as well as υ_{opt} in Fig.8 increase with β. Effectively, higher inertance not only enables higher inerter force but also supports the use of damping devices with higher damping coefficients which, ultimately, increases damping force leading to overall improved motion control.
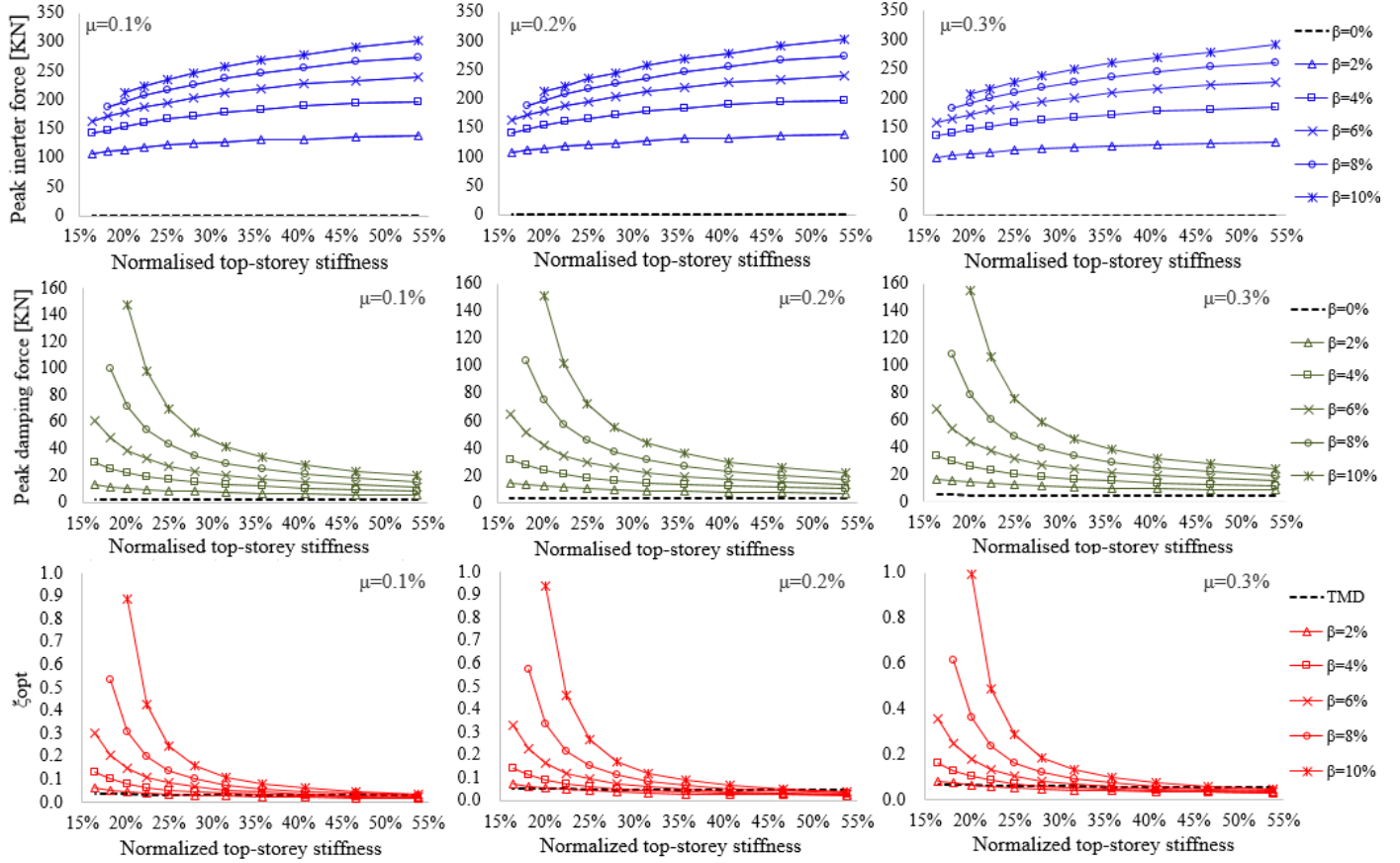

Fig. 9 Peak inerter force (upper row of panels), peak damping force (middle row of panels), and optimal damping ratios (lower row of panels) of TMDI-equipped structure for various mass ratios, μ, and inertance ratios, β, against lateral top-storey stiffness reduction.

Nevertheless, top-storey stiffness reduction has a prominently different effect between the inerter force and the damping force. Peak inerter force decreases as the top-storey softens at an increasing rate. On the contrary, damping force increases as the top-storey softens at a rate that becomes exponential for $\beta{\geq}6\%$. These trends indicate that top-storey stiffness reduction improves TMDI motion control performance through significant increase of the damping force but not of the inerter force. Notably, the achieved increase in damping force via top-storey softening does not come from an increase to the relative velocity at the ends of the damper, but to an increase of c_{opt} in Eq.(22). This can be appreciated by noting that the variation trends of ξ_{opt} with top-storey stiffness reduction in Fig. 9 are similar to those of υ_{opt} in Fig.8 and to peak damping force trends in Fig. 9. In this respect, top-storey stiffness reduction affects TMDI damping force in a similar manner as the increasing of inertance.

With regards to the actual values of peak TMDI forces attained for the case-study structure under the assumed wind intensity, it is seen that the inerter force is always larger than the damping force (for the herein considered β and μ inertial properties) and this difference is higher for larger inertance values and/or stiffer top-storey. The highest inerter force observed is of the order of 320kN (for β=10% and h=4.0m) which can be readily transferred to the host structure without requiring any out-of-ordinary connection and be safely accommodated by an adequately designed inerter device. Yet, top-storey stiffness reduction tends to balance off the difference between peak inerter and damping forces for fixed inertance resulting in a reduction to peak inerter force. For instance, the peak inerter force of 320kN drops to 225kN for β=10% through stiffness reduction by 35%. In this regard, top-storey softening is beneficial in containing peak inerter force.

Trading secondary mass to inertance and/or top-storey stiffness in performance-oriented design

Numerical results reported in Fig.8 suggest that the same structural performance, in terms of peak floor acceleration, can be achieved by using different sets of secondary design variables in $\mathbf{y_2}$ (i.e., secondary mass, inertance, and top-storey stiffness). This is an important consideration from the designer's viewpoint as it enables exchanging secondary mass (attached weight) to inertance and/or to top-storey stiffness within a performance-oriented design context (i.e., aiming to achieve a pre-set performance level). To illustrate this point and to quantify potential practical benefits, Fig. 10(a) and 10(b) plot optimal iso-performance curves on the TMDI inertial μ-β plane for fixed top-storey stiffness and for fixed performance, respectively.

Optimal damping coefficient, c_{opt}, and peak inerter force, F_b, and damping force, F_c, are reported for all optimal designs considered in the graphs. It is seen that all iso-performance curves have negative slope on the μ-β plane establishing the direct mass reduction/substitution effect endowed by the inerter to the TMDI and leading to overall more lightweight inertial dampers: a practically important advantage in designing new slender minimal-weight tall buildings. Nevertheless, trading mass to inertance for fixed top-storey stiffness, Fig. 10(a), comes at the cost of increased damping coefficient and force as well as increased inerter force. Further, significant increase to the inertance and to damping coefficient and force are required to achieve small performance improvements for fixed mass. Quantitatively, for μ=0.1% it takes, on average, increases of about 15% in inertance and 72% in damping coefficient, leading to an average increase of 31% of peak damping force, for every 1% of improvement of peak floor acceleration. Conveniently, these arduous requirements can be relaxed through minute top-storey softening as seen in Fig. 10(b). For μ=0.1%, the same performance can be achieved with reduced average required inertance, damping coefficient, and damping force by approximately 18%, 28%, and 25%, respectively, for every 2% reduction to the top-storey stiffness. As a final remark, top-storey softening further leads to attached mass reduction for fixed inertance to achieve a preset performance: Fig. 10(b) shows that 2% reduction of top-storey stiffness reduces the required mass ratio by about 0.1% corresponding to a 20ton TMDI weight reduction for the case-study building.
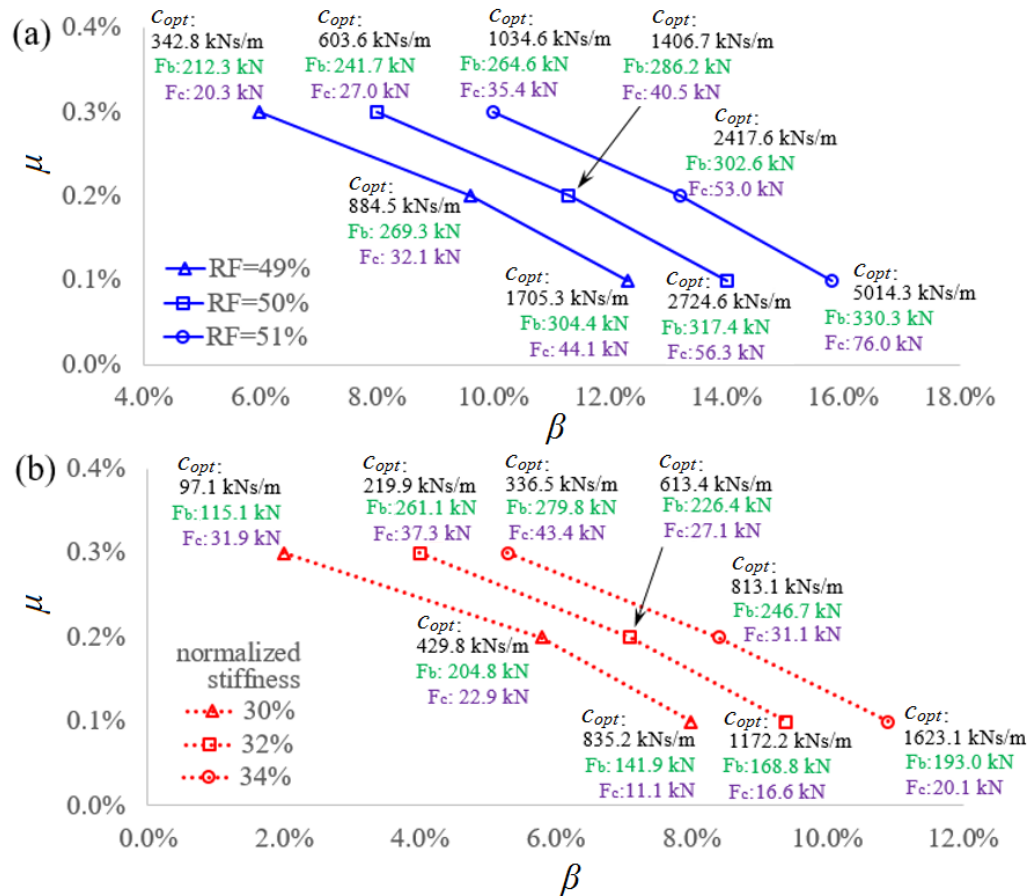
Fig.10 Quantification of mass-inertance-damping coefficient trade-off for (a) fixed normalized stiffness 38%, and (b) fixed performance RF=50%.

INFLUENCE OF BUILDING PROPERTIES TO FLOOR ACCELERATION PERFORMANCE

In this final section the influence of the inherent damping and r/c core stiffness of the case-study building to the performance of optimal-TMDI equipped structure is quantified, separately, through pertinent parametric analyses. The influence of these two building properties was deemed important to assess since: (a) accurate estimation of the inherent damping properties in tall buildings is a quite challenging task involving uncertainty (e.g., Spence and Kareem 2014) while it is known to affect significantly their response to wind excitation, (b) lateral r/c core stiffness is primarily defined from along-wind direction ultimate limit state design (e.g., Huang 2017) and, therefore, may vary independently from serviceability limit state design in the across-wind direction.

Influence of inherent structural damping modelling

To explore the influence of the inherent structural damping, the first mode damping ratio, ξ_1, of the case-study building is herein estimated using the following three different damping models proposed in the literature: $\xi_1 = 0.01 f_1$ (Jeary 1986), $\xi_1 = 0.002884/f_1 + 0.012856 f_1$ (Largomarsino 1993), and $\xi_1 =$

$0.0231f_1$ (Satake et al. 2003), where f_1 is the first structural natural frequency in Hz. Damping ratios for higher modes are taken the same as before as it is found that their influence is insignificant to structural performance. The coefficient of variation (COV= mean value over standard deviation) of the peak 32nd floor acceleration of optimal TMDI-equipped case-study structure with ξ_1 computed from the above three models is plotted in the upper panels of Fig. 11 as a function of the inertance and for various mass ratio μ and top-storey height H_{top} values.
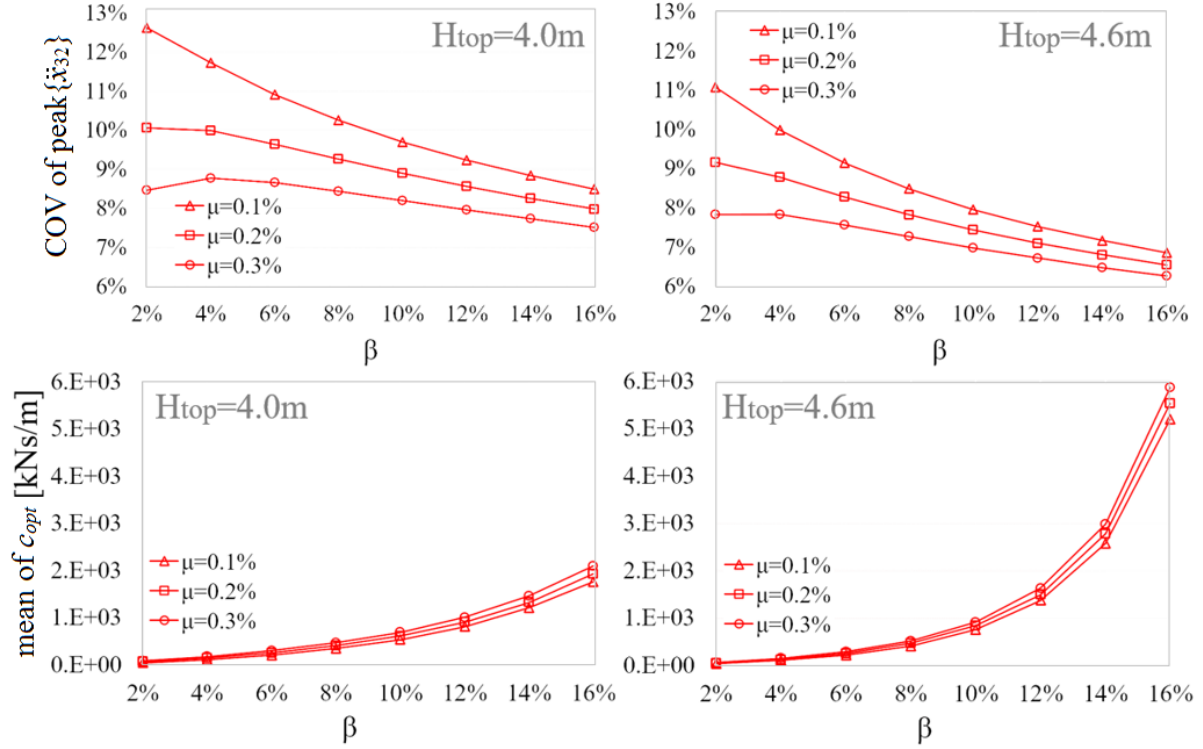

Fig.11 COVs of peak across-wind acceleration at 33rd floor (upper panels) and mean c_{opt} (lower panels) as functions of inertance ratio for three inherent damping models for various mass ratios and top-storey height.

It is observed that the significance of the influence of the assumed/estimated ξ_1 value to structural performance reduces with increased inertance and this reduction is larger as the mass ratio reduces. Interestingly, it is further seen that the influence of the inherent damping is less important as the top-storey softens. Finally, as β and H_{top} increase performance COV for different mass ratios converge. All the above trends can be readily attributed to the fact that c_{opt} values increase with inertance and top-storey softening as shown in the lower panels of Fig. 11. In this regard, the effect of the assumed ξ_1 value becomes less important in optimal TMDI-equipped tall buildings as inertance increases and/or top-storey softens due to the increased TMDI supplementary damping rendering the inherent damping modelling less critical in tall buildings design.

Influence of r/c core stiffness

Treating the structure in Fig.2 as the base-case, two variants of the case-study structure with r/c core lateral stiffness contribution uniformly reduced by 10% and 20% are considered. This is readily

achieved through the low-order model of the structure by multiplying the $\mathbf{K}_{CORE}$ term in Eq. (1) with reduction factors 0.9 and 0.8, respectively, while the perimetric MRF stiffness contribution remains the same. Figure 12 plots percentage reduction factor (RF) of peak 32nd floor acceleration of optimal TMDI-equipped structures over optimal TMD-equipped structures (β=0) with different core stiffness as function of top-storey stiffness reduction for μ=0.1% and for different β values.

It is seen that TMDI peak floor acceleration control capability deteriorates slightly compared to TMD capability as the relative stiffness contribution of the core reduces by about 1% for 10% r/c core stiffness reduction. Notably, this deterioration is independent of top-storey stiffness. These findings suggest that top floor optimal TMDIs are more efficient for tall buildings behaving closer to a flexural cantilever. It is, therefore, concluded that increasing lateral stiffness contribution of the r/c core as opposed to the MRFs to contain deformation demands in the along-wind direction facilitates controlling floor accelerations in the across-wind direction by means of TMDI.
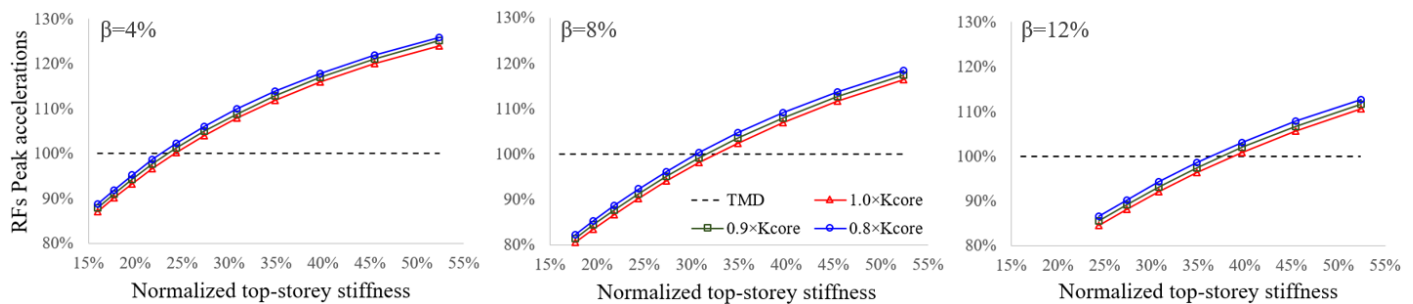

Fig. 12 Peak acceleration percentage reduction of 32nd floor for optimal TMDI-equipped versus optimal TMD-equipped structures with different r/c core contributions against lateral top-storey stiffness reduction for attached mass ratio μ=0.1%, and various inertance ratios.

CONCLUDING REMARKS

The effectiveness and advantages of using optimally tuned top-storey TMDIs in conjunction with an innovative local structural modification, i.e., top-storey lateral stiffness reduction, have been numerically explored for mitigating floor accelerations in the across-wind direction of slender core-frame high-rise buildings critical for serviceability design (occupants' comfort criteria). This has been accomplished by furnishing pertinent numerical data for a low-order top-storey-TMDI-equipped dynamical system capturing faithfully in-plane modal properties (mode shapes and natural frequencies) of a 34-storey square-plan core-frame benchmark building with softened top-floor through discontinuing the central r/c core and increasing the top-floor height. A novel optimal TMDI tuning problem has been formulated and numerically solved treating as design parameters TMDI properties and top-floor height aiming to minimize peak floor acceleration demands under across-wind excitation forces. These forces were modelled as a stationary spatially-correlated random field accounting for vortex shedding effects.

Numerical results obtained for different TMDI inertial properties (mass and inertance) and top-storey height have shown that improved structural performance in terms of peak floor acceleration and attached mass stroke are achieved by increasing inertance and/or by reducing top-storey stiffness for fixed TMDI attached mass, while no improved performance is achieved by the classical TMD (no inertance) with top-storey softening. In this regard, it was demonstrated, through the consideration of optimal TMDI design charts for fixed floor acceleration performance, that the required TMDI mass/weight can be reduced either by increasing inertance or by softening the top storey. This is deemed a rather advantageous consideration in the design of new structures. Still, it was found that mass reduction achieved through increased inertance *for a fixed target performance* increases the required damping and inerter forces exerted to the structure. However, these forces reduce for fixed attached mass and structural performance by exchanging inertance to top-storey softening. Thus, by leveraging inertance and top-storey stiffness, the proposed motion control solution can be judicially designed to exert overall balanced and relatively small amplitude additional forces in new structures in the gravitational (small added weight) and the horizontal directions. Additionally, it was shown that increase of the top-storey height lead to increased robustness of structural performance (floor acceleration) with respect to the optimal TMDI properties and as well as to the assumed inherent structural damping. Therefore, top-storey softening yields more robust TMDI designs to detuning effects as well as to inaccurate knowledge of structural properties. Lastly, it was seen that response acceleration performance of optimal TMDI-controlled structures improves by increasing the flexural contribution in coupled core-frame lateral load-resisting suggesting that increasing the core vis-à-vis frame resistance in meeting ultimate limit design criteria in the along-wind direction favors meeting serviceability design criteria in the across-wind direction.

Looking further into the case of existing tall/slender buildings, the herein reported numerical data suggest that the addition of a relatively soft top-storey housing a properly tuned lightweight TMDI is a potent retrofitting measure to enhance serviceability performance. In this manner, more stringent serviceability design requirements than those considered in the initial design due to site-specific climate change effects or changes to the surrounding built environment (i.e., increased wind exposure) can be achieved.

As a final remark, it is noted that throughout this work ideal linear inerter behaviour was assumed. Whilst inerter device prototypes do deviate from the ideal inerter element behaviour depending on the employed technology and the application-dependent frequency range of operation (e.g. Papageorgiou and Smith 2005, Swift et al. 2013), recent studies demonstrate that such deviations do not significantly influence the benefits of the inertance in dynamic vibration absorbers (e.g., Gonzalez-Buelga et al. 2016, Brzeski and Perlikowski 2017, Pietrosanti et al. 2019). Therefore, it is anticipated that the herein reported trends and conclusions are valid even for non-ideal inerter devices, although it is recognized that quantification of benefits and performance accounting for non-ideal inerter behaviour warrants further research work.

Wang Z and Giaralis A (2020) Top-storey softening for enhanced mitigation of vortex shedding induced vibrations in wind-excited optimal tuned mass damper inerter (TMDI)-equipped tall buildings, *Journal of Structural Engineering,* DOI: 10.1061/(ASCE)ST.1943-541X.0002838

DATA AVAILABILITY STATEMENT

All reported numerical data, computational models, and computer code produced during this study are available from the corresponding author by request.

REFERENCES

Brincker, R. and Ventura, C.E. (2015). *Introduction to Operational Modal Analysis*. John Wiley & Sons, Ltd, Chichester, UK.

Brzeski, P. and Perlikowski, P. (2017). "Effects of play and inerter nonlinearities on the performance of tuned mass damper." *Nonlinear Dyn.*, 88: 1027–1041.

Burton, M.D., Kwok, K.C.S, Hitchcock, P.A. and Denoon, R.O. (2006). Frequency dependence of human response to wind-induced building motion. Journal of Structural Engineering-ASCE, 132:296-303.

CEN (2005) European Standard EN 1991-1-4. Eurocode 1: Actions on structures, Part 4: wind actions. Committee for Standardization. Brussels, Belgium.

Charles, A. and Dennis Jr., J.E. (2003). *"Analysis of Generalized Pattern Searches."* SIAM Journal on Optimization. 13(3), 889–903.

Chopra, A.K. (2000). *Dynamics of Structures: Theory and Applications to Earthquake Engineering*, 2nd Edition, Prentice-Hall, U.S.

Ciampoli, M., and Petrini, F. (2012). "Performance-Based Aeolian Risk assessment and reduction for tall buildings." *Prob. Eng. Mech.,* 28:75–84.

Cluni, F., Gioffrè, M. and Gusella, V. (2013). "Dynamic response of tall buildings to wind loads by reduced order equivalent shear-beam models." *J. Wind Eng. Ind. Aerodyn.*, 123, 339–348.

Davenport, A.G. (1964). *"Note on the distribution of the largest value of a random function with application to gust loading."* Proc. of the Institution of Civil Engineers, 28(2), 187-196.

De Angelis, M., Perno, S. and Reggio, A. (2012). "Dynamic response and optimal design of structures with large mass ratio TMD." *Earthquake Eng. Struct. Dyn.*, 41, 41–60.

Den Hartog. (1947). *Mechanical vibrations.* McGraw-Hill, Inc., New York.

Dym, C.L. and Williams, H.E. (2007). "Estimating fundamental frequencies of tall buildings." *J. Struct. Eng.*, DOI: 10.1061/(ASCE)0733-9445(2007)113:10(1479), 1479-1483.

Elias, S. and Matsagar, V. (2014). "Wind response control of a 76-storey benchmark building installed with distributed multiple tuned mass dampers." *Journal of Wind and Engineering,* 11: 37-49.

Elias, S. and Matsagar, V. (2017). "Research developments in vibration control of structures using passive tuned mass dampers." *Annual Reviews in Control*, 44: 129-156.

Elias, S. and Matsagar, V. (2018). "Wind response control of tall buildings with a tuned mass damper." *Journal of Building Engineering*, 15:51-60.

Fang, J.Q., Jeary, A.P., Li, Q.S. and Wong, C.K. (1997). "Random damping in buildings and its AR model." *J. Wind Eng. Ind. Aerodyn.*, 79, 159–167.

Giaralis, A. and Taflanidis, A.A. (2015). "Reliability-based design of tuned-mass-damper-inerter

(TMDI) equipped stochastically support excited structures." *Proc., 12th Int. Conf. on Applications of Statistics and Probability in Civil Engineering,* T. Haukass, ed., paper #538, The University of British Columnbia, ISBN 978-0-88865-245-4.

Giaralis, A. and Petrini, F. (2017). "Wind-induced vibration mitigation in tall buildings using the tuned mass damper-inerter (TMDI)." *J. Struct. Eng.*, DOI: 10.1061/(ASCE)ST.1943-541X.0001863.

Giaralis, A. and Taflanidis, A.A. (2018). "Optimal tuned mass-damper-inerter (TMDI) design for seismically excited MDOF structures with model uncertainties based on reliability criteria." *Struct. Control Health Monitor.*, 25(2), DOI: 10.1002/stc.2082.

Gonzalez-Buelga, A., Lazar, I., Jiang, J.Z., Neild, S.A. and Inman, D.J. (2016). "Assessing the effect of nonlinearities on the performance of a Tuned Inerter Damper." *Struct. Control Health Monit.*, DOI: 10.1002/stc.1879.

Huang, M.F. (2017). *High-rise buildings under multi-hazard environment.* Singapore: Springer Nature.

Jeary, A.P. (1986). "Damping in tall buildings. A mechanism and a predictor." *Earth. Eng. Struct. Dyn.*, 14, 733-750.

Kareem, A., Kijewski, T. and Tamura, Y. (1999). "Mitigation of motions of tall buildings with specific examples of recent applications." *Wind Structures*, 2(3), 201-251.

Kwok, K.C.S, Hitchcock, P.A. and Burton, M.D. (2009). "Perception of vibration and occupant comfort in
wind-excited tall buildings." *J. Wind Eng. Ind. Aerodyn.*, 97, 368–380.

Lagomarsino, S. (1993). "Forecast models of damping and vibration periods of buildings." *J. Wind Eng. Ind. Aerodyn.*, 48, 221-239.

Liang, S., Liu, S., Li, Q.S., Zhang, L. and Gu, M. (2002). "Mathematical model of across-wind dynamic loads on rectangular tall buildings." *J. Wind Eng. Ind. Aerodyn.*, 90, 201-251.

Li, Q.S., Zhi, L.H., Tuan, A.Y., et al. (2011). Dynamic behavior of Taipei 101 Tower: Field measurement and numerical analysis. *J. Struct. Eng.*, 137, 143–155.

Marian, L. and Giaralis, A. (2013). "Optimal design of inerter devices combined with TMDs for vibration control of buildings exposed to stochastic seismic excitations." Proc,.11th ICOSSAR Int. Conf. on Structural Safety and Reliability, CRC Press, NY, 1025-1032.

Marian, L. and Giaralis, A. (2014). "Optimal design of a novel tuned mass-damper–inerter (TMDI) passive vibration control configuration for stochastically support-excited structural systems." *Prob. Eng. Mech.*, 38, 156–164.

Min, K.W., Kim, H.S., Lee, S.H., Kim, H. and Ahn, S.K. (2005). "Performance evaluation of tuned liquid column dampers for response control of a 76-story benchmark building." *Engineering Structures*, 27:1101-1112.

Nakaminami, S., Kida, H., Ikago, K. and Inoue, N. (2016). *"Dynamic testing of a full-scale hydraulic inerter-damper for the seismic protection of civil structures."* 7th International conference on advances in experimental structural engineering, pages 41-54. DOI:10.7414/7aese.T1.55.

Papageorgiou, C. and Smith, M.C. (2005). "Laboratory experimental testing of inerters." *Proc., 44th*

IEEE Conf. Decision Control, 3351-3356.

Petrini, F. and Ciampoli, M. (2012). "Performance-based wind design of tall buildings." *Structure & Infrastructure Engineering - Maintenance, Management*, Life-Cycle Design & Performance, 8(10), 954-966.

Petrini, F., Giaralis, A. and Wang, Z. (2020). "Optimal tuned mass-damper-inerter (TMDI) design in wind-excited tall buildings for occupants' comfort serviceability performance and energy harvesting." *Engineering Structures*, 204:109904. DOI: 10.1016/j.engstruct.2019.109904.

Pietrosanti, D., De Angelis, M. and Giaralis, A. (2019). "Experimental study of nonlinear dynamic response of SDOF system equipped with tuned mass damper inerter (TMDI) tested on shaking table under harmonic excitation." *Journal of Sound and Vibration*, under review.

Ruiz, R., Taflanidis, A.A., Giaralis. A. and Lopez-Garcia, D. (2018). "Risk-informed optimization of the tuned mass-damper-inerter (TMDI) for the seismic protection of multi-storey building structures." *Eng. Struct.*, 177: 836-850.

Samali, B., Mayol, E., Kwok, K.C.S., Mack, A. and Hitchcock, P. (2004). "Vibration control of the wind-excited 76-story benchmark building by liquid column vibration absorbers." *Journal of Engineering Mechanics-ASCE.*, 130:478-85.

Satake, N., Suda, K., Arakawa, T. and Tamura, Y. (2003). "Damping evaluation using full-scale date of building in Japan." *J. Struct. Eng.*, DOI: 10.1061/(ASCE)0733-9445(2003)129:4(470), 470-477.

Smith, M.C. (2002). "Synthesis of Mechanical Networks: The Inerter." *IEEE Trans. Automat. Control*, 47(10), 1648-1662.

Soong, T.T. and Grigoriu, M. (1993). *Random vibration of mechanical and structural systems*, Prentice-Hall, U.S.

Spence, S.M.J. and Kareem, A. (2014). "Tall buildings and damping: A concept-based data-driven model." *J. Struct. Eng.*, DOI: 10.1061/(ASCE)ST.1943-541X.0000890.

Swift, S.J., Smith, M.C., Glover, A.R., Papageorgiou, C., Gartner, B. and Houghton, N.E. (2013). "Design and modelling of a fluid inerter." *Intern. J. Control*, 86(11), 2035–2051.

Taflanidis, A.A., Giaralis, A. and Patsialis, D. (2019). "Multi-objective optimal design of inerter-based vibration absorbers for earthquake protection of multi-storey building structures." *Journal of the Franklin Institute.* DOI: 10.1016/j.jfranklin.2019.02.022.

Taranath S.B. (2017). *Tall Building Design, Steel, Concrete, and Composite Systems*. CRC Press.

Tse, K., Kwok, K., and Tamura, Y. (2012). "Performance and Cost Evaluation of a Smart Tuned Mass Damper for Suppressing Wind-Induced Lateral-Torsional Motion of Tall Structures." *J. Struct. Eng.,* 138(4): 514-525.

Zhang, Y., Li, L., Guo, Y. and Zhang, X. (2018). "Bidirectional wind response control of 76-story benchmark building using active mass damper with a rotating actuator." *Structural Control and Health Monitoring*, 25:e2216.